

A spatial multiscale mathematical model of *Plasmodium vivax* transmission

Shoshana Elgart¹, Mark B. Flegg², Somya Mehra³, and Jennifer A. Flegg³

¹*Laurel Springs School, Ojai, California, United States*

²*School of Mathematics, Monash University, Melbourne Australia*

³*School of Mathematics and Statistics, The University of Melbourne, Parkville, Australia*

Abstract

The epidemiological behavior of *Plasmodium vivax* malaria occurs across spatial scales including within-host, population, and metapopulation levels. On the within-host scale, *P. vivax* sporozoites inoculated in a host may form latent hypnozoites, the activation of which drives secondary infections and accounts for a large proportion of *P. vivax* illness; on the metapopulation level, the coupled human-vector dynamics characteristic of the population level are further complicated by the migration of human populations across patches with different malaria forces of (re-)infection. To explore the interplay of all three scales in a single two-patch model of *Plasmodium vivax* dynamics, we construct and study a system of eight integro-differential equations with periodic forcing (arising from the single-frequency sinusoidal movement of a human sub-population). Under the numerically-informed ansatz that the limiting solutions to the system are closely bounded by sinusoidal ones for certain regions of parameter space, we derive a single nonlinear equation from which all approximate limiting solutions may be drawn, and devise necessary and sufficient conditions for the equation to have only a disease-free solution. Our results illustrate the impact of movement on *P. vivax* transmission and suggest a need to focus vector control efforts on forest mosquito populations. The three-scale model introduced here provides a more comprehensive framework for studying the clinical, behavioral, and geographical factors underlying *P. vivax* malaria endemicity.

1 Introduction

Malaria is one of the most significant sources of morbidity and mortality across the world, resulting in nearly 250 million cases and accounting for over 60,000 deaths in 2021 alone [31]. The disease is particularly dangerous to young children (likely accounting for over 7% of all deaths in children under five) and to persons with compromised immune systems [24, 28].

Global efforts towards malaria elimination have refocused attention on disease caused by *Plasmodium vivax*, a malaria parasite responsible for a significant fraction of recurring blood-stage infections. *P. vivax* infections are characterized by the presence of hypnozoites

– latent forms of the *Plasmodium* sporozoites inoculated by the bites of infectious *Anopheles* mosquitoes – in host hepatocytes. Certain hypnozoites may *activate* after initial primary infections, causing malaria relapses in which the host may both experience blood-stage infection symptoms and is liable to transmit malaria to additional mosquitoes, thus significantly increasing the number of secondary cases that a primary case may give rise to [43]. Current anti-hypnozoital pharmaceutical interventions (chiefly the 8-aminoquinoline drugs primaquine and tafenoquine) are limited in their efficacy due to the risk for erythrocyte rupture in individuals with G6PD deficiency, emerging parasite resistance, and lack of funding for treatment availability in the private sector [9, 14, 33].

In the regions of Southeast Asia where *P. vivax* are highly prevalent, even small-scale spatial behavior is known to play a crucial role in disease transmission. In Cambodia, for example, where over 90% of malaria incidence involves *P. vivax* parasites, the majority of remaining endemic districts are isolated from urban areas and situated in proximity to tropical forests [13]. Owing to high humidity and seasonal floods, these forests are typically characterized as zones of severe prevalence among *Anopheles* populations, particularly when compared with nearby villages, where mosquitoes are targeted with long-lasting insecticidal nets, residual spraying, and other interventions [20]. Mobile groups (often termed “forest-goers”) who migrate between lower-transmission villages and high-transmission forests are considered to be at highest risk for contracting – and spreading – malaria, with the residual endemicity in forest-adjacent villages often attributed to the movement of forest-goers [8, 13, 34]. Similar patterns of movement-based transmission have been observed in neighboring Thailand, Laos, and Vietnam [34].

A number of spatial or *P. vivax* within-host mathematical models have been posed to describe malaria epidemiological dynamics and predict transmission. Since the model we present in this paper unifies the spatial and within-host representations, we discuss previous work most relevant to ours from both categories below.

We begin with spatial malaria models (e.g., [2, 4, 15, 29, 35, 37]) which either represent a vector-borne disease in general or specifically focuses on *Plasmodium falciparum* dynamics (this simplifies the model structure by rendering the inclusion of within-host dynamics less necessary). The articles [4, 37, 35] extend the SI (susceptible-infectious) Ross-Macdonald model to several patches. In particular, Prosper et al. [35] analyzes a two-patch model, and the works Auger et al. [4], Rodríguez and Torres-Sorando [37] study general n -patch models using arbitrary-large systems of ordinary differential equations (ODEs). In contrast to the original SI model framework, some spatial models represent human and mosquito populations in SEIR (susceptible-exposed-infectious-recovered) and SEI frameworks, respectively, so as to incorporate the significant latency period in malaria infections [15]. Non-ODE spatial models include a two-patch reaction-diffusion system and a numerical process-based model [2, 29]. Some models specify a residence patch for each individual or focus on long-period, long-distance movement [35, 37]. A large proportion of studies construct autonomous nonlinear ODE models, which are then analyzed using traditional methods (i.e., a linear stability analysis yielding bounds or explicit values for the models’ R_0) [4, 15, 37, 35].

Models representing *P. vivax* are generally rare, since the significance of the hypnozoite reservoir suggest that such models need a within-host component. White et al. [43] introduced a large ODE model (of up to 102 equations) with host compartments of the form S_i, I_i , where individuals in S_i or I_i carry exactly i hypnozoites, and numerically simulated

the model to yield results on *P. vivax* epidemiology. Mehra et al. [26] devised a framework for modeling both short-latency tropical and long-latency temperate malaria strains in a single host, representing hypnozoite accrual, activation, and clearance, as well as primary infection dynamics, through an open network of $\cdot/M/\infty$ (infinitely-many) server queues with batch arrivals. A probability generating function (PGF) is then derived to encapsulate the within-host dynamics associated with the individual in question. A population-level model was later built around this framework in Anwar et al. [3].

In this paper, we propose and analytically study the first mathematical model combining *P. vivax* within-host and metapopulation dynamics. We further extend the framework devised in Anwar et al. [3] and Mehra et al. [26], generating a two-patch model where the human population is divided into moving and non-moving individuals. Assuming that moving individuals' migration patterns align, we derive a system of eight integro-differential equations for the human-vector populations. We proceed to study the limiting equations of the system analytically using the ansatz that solutions are limit-periodic, the assumption that mean population movement is sinusoidal with rapid frequency, and the additional assumption that patch populations see very small rates of change. We structure the paper as follows: In Section 2, we introduce the model, adapt the within-host framework in Mehra et al. [26] to derive our system of metapopulation-level equations, and consider the constant force of reinfection case. In Section 3, we present our analytical and numerical results before providing concluding remarks in Section 4.

2 Model development

We introduce spatial dynamics into the multi-scale *Plasmodium vivax* framework developed in [3]. A representative schematic of the model is presented in Figure 1a.

2.1 Spatial patch model

In the general case, we distribute our collection of individuals and *Anopheles* mosquitoes across an arbitrary number of n distinct patches (blue hexagons). Metapopulation movement between patches takes the form of traversing a connected sub-graph of \mathbb{Z} with n vertices representing the patches (Figure 1a). Each Patch i contains a local population of mosquitoes, \mathcal{Q}_i . We denote the set of patches containing permanent human settlement – so-called “village patches” below – by $J \subset [1, n]$. In Figure 1a village patches are represented by a brown border around their present populations and placed on the left side of the respective patches whilst populations on non-village patches are placed on the right side of their patch with a green border.

Every patch $i \in J$ is the permanent residence of two subclasses of humans: moving humans (\mathcal{M}_i) and non-moving humans (\mathcal{N}_i), as shown connected to each respective patch in Figure 1a. In particular, we define \mathcal{M}_i to represent the subpopulation of humans residing on Patch i who are mobile and regularly travel to a different patch and define \mathcal{N}_i as the subpopulation of humans who do not travel beyond their village. Viewing \mathcal{N}_i and \mathcal{M}_i as *sets* of humans we define the population

$$\mathcal{H}_i := \mathcal{N}_i \cup \mathcal{M}_i, \tag{1}$$

the set of all humans with permanent residence on Patch i . The proportion that each subpopulation forms of the total Patch i population is represented without calligraphic font; $0 < M_i \leq 1$ and $N_i = 1 - M_i$, where

$$M_i := \frac{|\mathcal{M}_i|}{|\mathcal{H}_i|}, \quad N_i := \frac{|\mathcal{N}_i|}{|\mathcal{H}_i|}. \quad (2)$$

This is motivated by the studies Kunkel et al. [23] and Sandfort et al. [39], which found that most movement between areas with high and low malaria transmission in Cambodia is dominated by a single sub-population, typically consisting of younger men working as loggers or engaged in farming activities.

We focus most of our analysis in this paper on the simplest version of this patch model, the $n = 2$ case of a “village–forest” model (Figure 1b) describing the situation in which humans travel between an area of high settlement and low *Anopheles* density (Patch 1, a “village” location) to an area of low settlement and high *Anopheles* density (Patch 2, a “forest” location). We consider interactions between a single human population \mathcal{H} with permanent residence on Patch 1 (separated into a moving set of humans \mathcal{M} and a non-moving set of humans \mathcal{N}) and two sets of static mosquito populations \mathcal{Q}_1 and \mathcal{Q}_2 , associated with Patch 1 and Patch 2, respectively.

Analogously to the n -patch case, we define the quantities

$$\begin{aligned} M &:= \frac{|\mathcal{M}|}{|\mathcal{H}|}, & N &:= \frac{|\mathcal{N}|}{|\mathcal{H}|} \\ Q_1 &:= \frac{|\mathcal{Q}_1|}{|\mathcal{H}|}, & Q_2 &:= \frac{|\mathcal{Q}_2|}{|\mathcal{H}|}, \end{aligned} \quad (3)$$

such that M, N represent the proportion that the moving and non-moving populations, respectively, form of the total human population, while Q_1, Q_2 represent the sizes of the village and forest mosquito populations, respectively, relative to the human population.

The choice of qualifiers “forest” and “village” is motivated by studies exploring the epidemiological dynamics that result when individuals in South and Southeast Asia travel between forested areas where malaria is endemic and neighboring villages where malaria is largely suppressed [23, 36, 39].

We make the following simplifying assumptions in our two-patch model:

- (i) Only humans can move between patches, while mosquitoes remain on a single patch. This assumption is motivated by Auger et al. [4] and by estimates of *Anopheles* dispersal ranges, which have been found to be below a kilometer on average [27, 38].
- (ii) The moving group \mathcal{M} moves deterministically at the time-dependent, periodic rates $r_1(t)$ (from Patch 1 to Patch 2) and $r_2(t)$ (from Patch 2 to Patch 1).
- (iii) Each individual moving person is assumed to migrate in discrete jumps from one patch to the next. The sequence of transitions governing this movement is assumed to be time-periodic. We assume that each individual continues this periodicity of movement even throughout periods of malaria infection, a reasonable hypothesis in locations where asymptomatic cases dominate prevalence, such as Southeast Asia [6, 41].

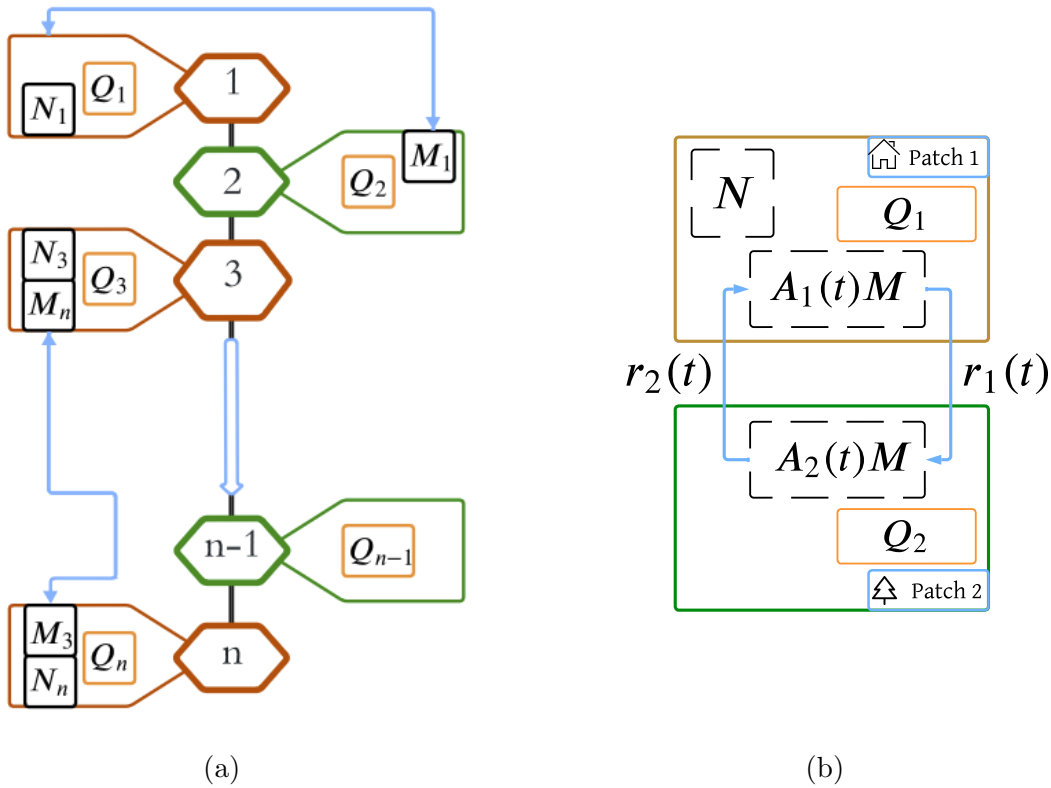


Figure 1: (a) Diagram of the n -patch model at a certain time t (not including inter-compartment interactions). Patches 2 and $n-1$ are “forest patches” (outlined in green) while Patches 1, 3, and n are “village” patches (outlined in brown). Each patch i is associated with a mosquito population Q_i (outlined in orange), while all village patches $j \in J \subset [1, n]$ contain a non-moving human population N_j . Light blue arrows indicate the movement of a group of individuals within M_k , $k \in J$, traveling from their patch (k) of permanent residence to a different patch (arrows are two-sided to indicate that moving individuals may return). (b) Diagram of the two-patch model at some time t . The proportions of moving individuals on Patches 1, 2, respectively, are $A_1(t)$, $A_2(t)$. Unlike Patch 1, Patch 2 does not contain *permanent* human residents, and thus has no non-moving individuals.

- (iv) We assume that the Q_1 population is much smaller than the Q_2 population (i.e., $Q_1 \ll Q_2$). Moreover, we suppose that $Q_1 + Q_2 < 1$ (from White et al. [43], which places the mean mosquito-to-human ratio in a homogeneous location at under 0.6), and that the death rate of Patch 2 mosquitoes is far lower than that of Patch 1 mosquitoes.
- (v) Immigration is not included, meaning that the total number of humans is constant over time. We further assume that both $|\mathcal{M}|$ and $|\mathcal{N}|$ are considerable, which allows us to define the total number of individuals on a patch as a continuous function of time and assume deterministic dynamics for the population as a whole (even as individual primary infection and hypnozoite dynamics remain stochastic).

Under assumption (ii), we have that

$$\frac{dA_1}{dt} = -r_1(t)A_1 + r_2(t)A_2 = -\frac{dA_2}{dt}. \quad (4)$$

Since $A_1(t) + A_2(t) = 1$, both $A_1(t)$ and $A_2(t)$ are periodic non-constant functions for all initial conditions by Floquet's theorem [11]. Moreover, as $r_1(t), r_2(t) > 0$, $A_1(t), A_2(t)$ lie between 0 and 1 for all t . We choose the initial conditions $A_1(0) = u + v, A_2(0) = 1 - u - v$, and let $r_1(t) = v\omega \sin(\omega t), r_2(t) = -v\omega \sin(\omega t)$, such that

$$\begin{aligned} A_1(t) &= u + v \cos(\omega t), \\ A_2(t) &= 1 - u - v \cos(\omega t). \end{aligned} \quad (5)$$

for parameters u, v, ω , where ω is in the units of days⁻¹. We assume that $0 < |v| \ll 0.5 < u < 1$ and $u + |v| < 1$, which implies that the average density of moving individuals on Patch 1 exceeds that on Patch 2.

2.1.1 Infection status within patches

We briefly introduce some additional notation on the population-level, which will be referenced in the within-host analysis below. The force of reinfection (FORI), denoted $\lambda_i(t)$, is unique to a patch as it is directly dependent on the proportion of infectious mosquitoes resident on that patch.

We will use I_M, I_N to denote the compartments of blood-infected moving and non-moving individuals, respectively. The liver-infected compartments L_M, L_N – containing individuals with latent hypnozoites, but no active blood infections – are defined similarly. All other individuals are placed into the susceptible S_M compartment (if moving) or the S_N compartment (if non-moving). In particular, $M = I_M + L_M + S_M$ and $N = I_N + L_N + S_N$. The proportion of infectious mosquitoes on Patch i will be given by $I_{mi}, i \in \{1, 2\}$.

2.2 Within-host model

We begin by capturing within-host dynamics for an arbitrary non-moving individual. Here, we apply the analysis and resulting probability generating function (PGF) derived in [26], which describes the stochastic primary infection and hypnozoite-related processes in the

case of an individual in a homogeneous environment, as a function of the FORI associated with the environment.

Considering a single hypnozoite established in the host immediately after an infective bite at time $t = 0$, we let the initial *establishment* state of the hypnozoite in a host hepatocyte be H . From Equation (13) in [26], the probability $p_H(t)$ that a single short-latency hypnozoite established at time 0 is in state H at time t satisfies

$$p_H(t) = e^{-(\alpha+\mu)t}. \quad (6)$$

An established hypnozoite may activate, transitioning to a state A at rate α and causing a relapse infection that is cleared at rate γ (at which point the hypnozoite enters a cleared state C). From Equations (14)-(15) in [26], the probabilities $p_A(t), p_C(t)$ that a hypnozoite established at time 0 is activated or cleared, respectively, at time t are given by

$$\begin{aligned} p_A(t) &= \frac{\alpha}{\alpha + \mu - \gamma} (e^{-\gamma t} - e^{-(\alpha+\mu)t}), \\ p_C(t) &= \frac{\alpha}{\alpha + \mu} (1 - e^{-(\alpha+\mu)t}) - \frac{\alpha}{\alpha + \mu - \gamma} (e^{-\gamma t} - e^{-(\alpha+\mu)t}). \end{aligned} \quad (7)$$

Alternatively, an established hypnozoite may die, transitioning to a state D at rate μ . By Equation (16) in [26], the probability $p_D(t)$ that a hypnozoite established at time 0 is dead at time t is given by

$$p_D(t) = \frac{\mu}{\alpha + \mu} (1 - e^{-(\alpha+\mu)t}). \quad (8)$$

In addition to defining states for each inoculated hypnozoite, we refer to an active primary infection as being in state P . Similarly to relapses, primary infections are cleared at rate γ , transitioning to a state PC . This chain of transitions is illustrated in Figure 2.

We assume that the time-dependent random variables representing the state of each hypnozoite dormant within the host are independent and identically-distributed (e.g., the probabilities in (6), (7),(8) apply to each hypnozoite contained in the host). When a vector infects the individual with *P. vivax* parasites, the individual receives both a primary infection and an inoculation of h hypnozoites (with the probability mass function for h being geometrically-distributed, and with h having expected value ν and associated state space $[0, \infty) \cup \mathbb{Z}$), see Figure 2.

2.3 Probability-generating functions for within-host dynamics within moving and non-moving individuals

The rate of infective bites on Patches 1 and 2 on the interval $[0, t]$ are modeled by non-homogeneous Poisson processes with rates $\lambda_1(t), \lambda_2(t)$ respectively. We assume that hypnozoite inoculation is instantaneous.

We denote the number of hypnozoites in the established, activated, cleared, and dead states by $\mathcal{N}_H(t), \mathcal{N}_A(t), \mathcal{N}_C(t), \mathcal{N}_D(t)$, respectively, and also denote the number of primary infections and cleared infections by $\mathcal{N}_P(t)$ and $\mathcal{N}_{PC}(t)$, respectively.

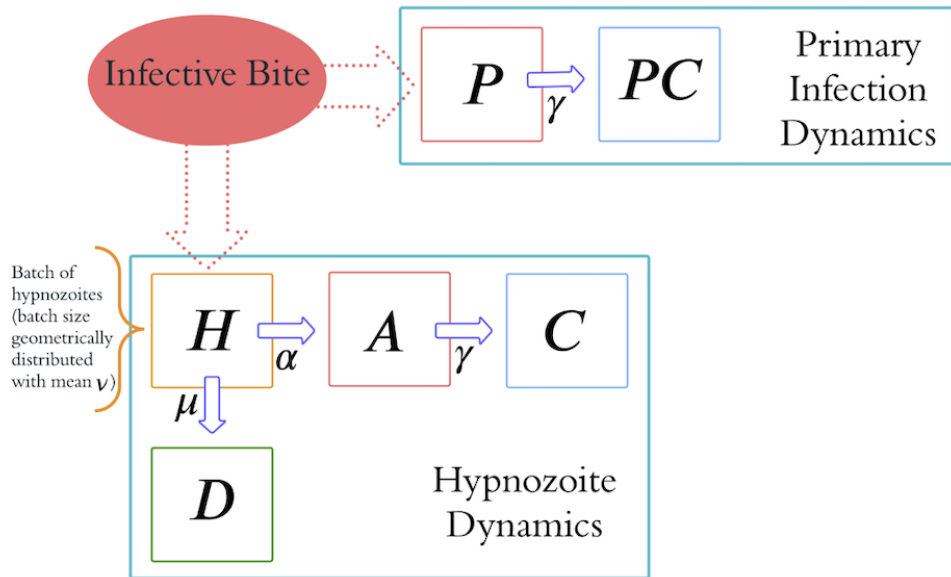


Figure 2: Schematic representation of primary infection and within-host dynamics for a single individual, based on the analysis in [26]. An infective bite (top left) establishes a primary infection (in within-host compartment P) and a batch of hypnozoites (initially in latent within-host compartment H), which activate at rate α and die at rate μ , moving to within-host compartments A , D respectively. Both primary infections and secondary infections caused by activated hypnozoites clear at rate γ , moving to compartments PC , C , respectively.

Letting $F' = \{H, A, C, D, P, PC\}$ and $F = \{H, A, C, D\}$, by [26], the PGF yielding within-host dynamics for individuals in \mathcal{N} is given by

$$G_N(z_H, z_A, z_C, z_D, z_P, z_{PC}) := \mathbb{E}\left[\prod_{f \in F'} z_f^{\mathcal{N}_f(t)}\right] = \exp \int_0^t \left(\lambda_1(\tau) \left(\frac{(z_P e^{-\gamma(t-\tau)} + (1 - e^{-\gamma(t-\tau)}) z_{PC})}{1 + \nu \left(1 - \sum_{f \in F} z_f \cdot p_f(t - \tau)\right)} \right) - 1 \right) d\tau. \quad (9)$$

We now extend the above PGF for an individual in the moving group \mathcal{M} . To the latter individual, we associate a discrete piecewise-continuous *movement function* $\mathcal{B}_j(t) := \mathbb{R}^+ \rightarrow \{0, 1\}$, equal to 1 when the individual j is on Patch 1 (their home village) and to 0 otherwise. The derivation of the PGF characterizing within-host dynamics for the moving individual is unaltered up to a change in the force-of-reinfection experienced by the individual. The within-host PGF for an individual in \mathcal{M} with movement function $\mathcal{B}_j(t)$ thus becomes

$$G_M^{(j)}(z_H, z_A, z_C, z_D, z_P, z_{PC}) := \mathbb{E}\left[\prod_{f \in F'} z_f^{\mathcal{N}_f(t)}\right] = \exp \int_0^t \left[\mathcal{B}_j(\tau) \lambda_1(\tau) + (1 - \mathcal{B}_j(\tau)) \lambda_2(\tau) \right] \left[\frac{(z_P e^{-\gamma(t-\tau)} + (1 - e^{-\gamma(t-\tau)}) z_{PC})}{1 + \nu \left(1 - \sum_{f \in F} z_f \cdot p_f(t - \tau)\right)} - 1 \right] d\tau. \quad (10)$$

Each function $\lambda_i(t), i \in \{1, 2\}$ depends both on the proportion of infectious mosquitoes (relative to the entire mosquito population) and on the mosquito-to-human ratio on this patch. We write

$$\begin{aligned} \lambda_1(t) &= ab \cdot \frac{I_{m1}(t)}{Q_1} \cdot \frac{Q_1}{(N + (u + v \cos \omega t) M)} = \frac{ab I_{m1}(t)}{(N + (u + v \cos \omega t) M)}; \\ \lambda_2(t) &= ab \cdot \frac{I_{m2}(t)}{Q_2} \cdot \frac{Q_2}{M((1 - u) - v \cos \omega t)} = \frac{ab I_{m2}(t)}{M((1 - u) - v \cos \omega t)} \end{aligned} \quad (11)$$

by (5). Here, the FORI on Patch $i, i \in \{1, 2\}$, is the product of ab – which represents the mean mosquito bite rate a (in days⁻¹) across both patches multiplied by the mean probability of mosquito-to-human transmission b – with the proportion of infectious mosquitoes on Patch i , and the mosquito-to-human ratio on Patch i . Using the shorthands

$$f(t) := \frac{-e^{-\gamma t} - \nu p_A(t)}{1 + \nu p_A(t)}$$

and

$$g(t) := \frac{-e^{-\gamma t} - \nu p_A(t) - \nu p_H(t)}{1 + \nu p_A(t) + \nu p_H(t)},$$

we apply (9) and (10) to characterize the probabilities that individual humans are liver- or blood-infected. We note here that, by Equation (51) in [26], $|f(t)|$ captures the probability that an infective bite at time 0 leads to a blood-stage infection at time t . Similarly, $|g(t)|$ captures the probability that an infective bite at time 0 leads to either a blood-stage or a liver-stage infection at time t .

Following [3], we note that the probability of an individual in \mathcal{N} to be blood-infected (i.e., in the compartment I_N) is given by

$$1 - G_N(z_H = 1, z_A = 0, z_C = 1, z_D = 1, z_P = 0, z_{PC} = 1) = 1 - \exp\left(\int_0^t \lambda_1(\tau) f(t - \tau) d\tau\right). \quad (12)$$

Moreover, the probability that an individual in \mathcal{M} characterized by movement function $\mathcal{B}_j(t)$ is blood-infected (i.e., in I_M) can be written as

$$G_M^{(j)}(z_H = 1, z_A = 0, z_C = 1, z_D = 1, z_P = 0, z_{PC} = 1) = 1 - \exp\left(\int_0^t (\mathcal{B}_j(\tau)\lambda_1(\tau) + (1 - \mathcal{B}_j(\tau))\lambda_2(\tau)) f(t - \tau) d\tau\right). \quad (13)$$

Similarly, the probability that an individual in \mathcal{N} belongs to L_N (the liver-infected stationary population) at time t is given by

$$G_N(z_H = 1, z_A = 0, z_C = 1, z_D = 1, z_P = 0, z_{PC} = 1) - G_N(z_H = 0, z_A = 0, z_C = 1, z_D = 1, z_P = 0, z_{PC} = 1) = \exp\left(\int_0^t \lambda_1(t) f(t - \tau) d\tau\right) - \exp\left(\int_0^t \lambda_1(t) g(t - \tau) d\tau\right), \quad (14)$$

while the probability that an individual in \mathcal{M} migrating with the same movement function as above belongs to L_M (liver-infected migratory population) at time t is

$$G_M^{(j)}(z_H = 1, z_A = 0, z_C = 1, z_D = 1, z_P = 0, z_{PC} = 1) - G_M^{(j)}(z_H = 0, z_A = 0, z_C = 1, z_D = 1, z_P = 0, z_{PC} = 1) = \exp\left(\int_0^t (\mathcal{B}_j(\tau)\lambda_1(\tau) + (1 - \mathcal{B}_j(\tau))\lambda_2(\tau)) f(t - \tau) d\tau\right) - \exp\left(\int_0^t (\mathcal{B}_j(\tau)\lambda_1(\tau) + (1 - \mathcal{B}_j(\tau))\lambda_2(\tau)) g(t - \tau) d\tau\right). \quad (15)$$

We note that, in order for differential equations to be used in describing population dynamics, the number of humans in the population must be modeled as a continuum. In other words, there must exist a bijection between the space of moving humans and the closed interval $[0, M]$. We use this in Section 2.4.1 to tie the movement functions of each individuals $i \in \mathcal{M}$ to the functions $A_1(t), A_2(t)$.

Figure 3 illustrates the probabilities (13) and (15) for two moving individuals migrating with different periods relative to the population's mean period of movement ($2\pi/\omega$). We note that the slow-moving individual exhibits far greater amplitude of oscillations in infection probability than the rapidly-moving individual, and that both individuals' probabilities of becoming liver- and blood-infected are periodic functions with multiple frequencies. Oscillations in infection probability vary across time, with variations coinciding with changes in the rate of mean population migration.

In Section 2.4, we will use the probabilities derived above (particularly (12) and (13)) to formulate population-level equations governing the time evolution of infected humans.

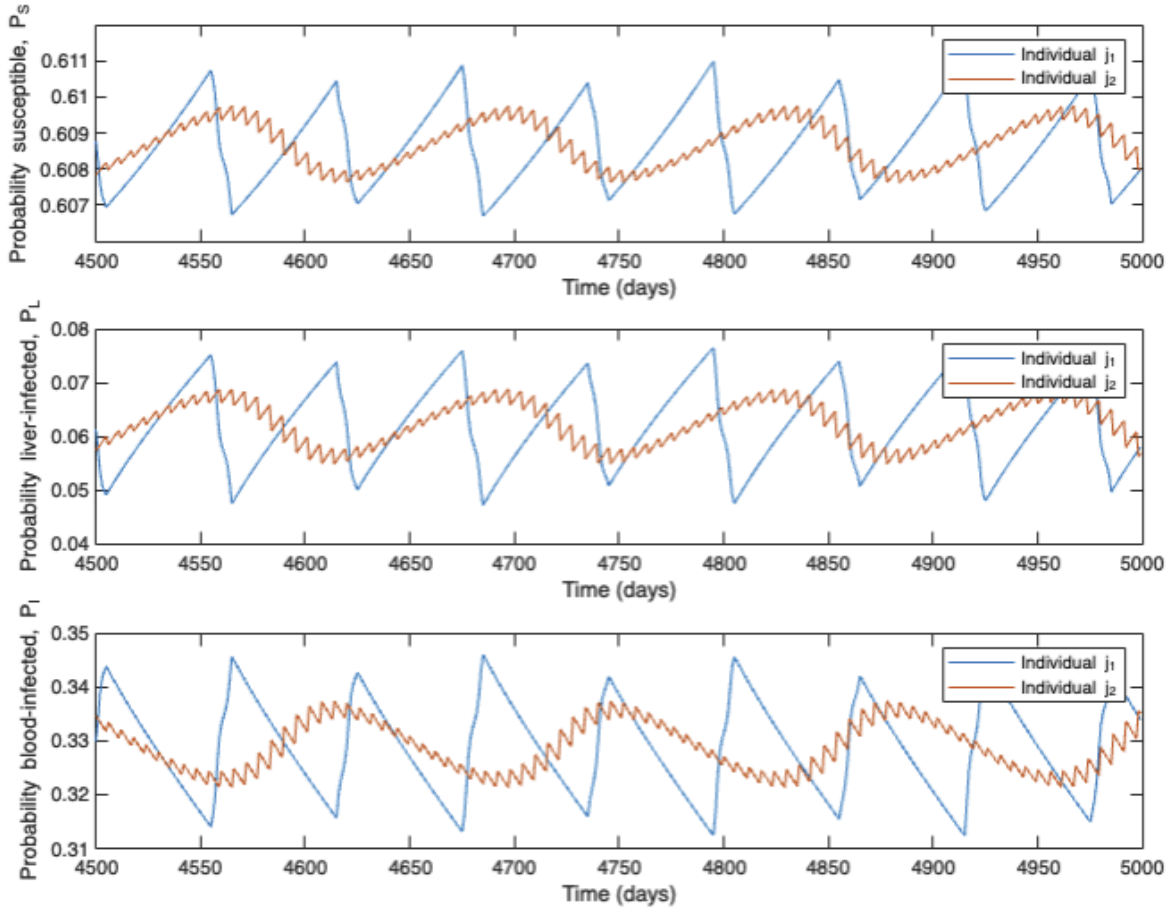


Figure 3: Comparison of probabilities for a slow-moving ($j_1 \in \mathcal{M}$) and fast-moving ($j_2 \in \mathcal{M}$) individual to be susceptible (P_S), liver-infected (P_L), and blood-infected (P_I), respectively, at time $t \in [4500, 5000]$. We assume the parameter values to be those in Table 1, so that the mean period of population movement is $2\pi/\omega = 2\pi$ days. The fast-moving individual (brown lines) switches patch at a frequency of 1 day^{-1} , above the population mean frequency; the slow-moving individual (blue lines) travels at a frequency of $\frac{1}{60} \text{ days}^{-1}$, below the population mean frequency. Probabilities are derived from Equations (11), (13), and (15).

2.4 Population-level model

We now turn from the individual-level scale to the population-level one. In our model, we do not explicitly represent population-level interactions between the six human compartments defined in Section 2.2. Rather, we use the transitions between compartments embedded inside the within-host model to characterize all compartment densities as functions of the two forces of reinfection (11).

	Definition	Value	Source
a	Mean daily mosquito bite rate	0.21 days ⁻¹	[16]
b	Probability of mosquito to human transmission	0.5*	[40]
c	Probability of human to mosquito transmission	0.23*	[7]
g_1	Patch 1 mosquito demography rate	0.1 days ⁻¹	[17]
g_2	Patch 2 mosquito demography rate	0.08 days ⁻¹	[42]
n	Mosquito sporogyny rate	1/12 days ⁻¹	[17]
Q_1	Proportion of mosquitoes on Patch 1 relative to number of humans	0.116*	[32, 43]
Q_2	Proportion of mosquitoes on Patch 2 relative to number of humans	0.464*	[32, 43]
u	$A(0)$, where $A(t) = u + v \cos \omega t$ is the density of moving humans on Patch 1 at time t	0.5 days ⁻¹	Arbitrary, later varied
v	$A(0) - A(\pi/2)$	-0.25 days ⁻¹	Arbitrary, later varied
ω	$(2\pi) \times$ the frequency of human movement	1 day ⁻¹	Chosen due to the travel patterns mentioned in [5]
α	Hypnozoite activation rate	1/332 days ⁻¹	[43]
μ	Hypnozoite death rate	1/425 days ⁻¹	[43]
γ	Blood-infection clearance rate	1/60 days ⁻¹	[10]
ν	Mean number of hypnozoites established in a bite	5*	[44]

Table 1: List of baseline values for model parameters, used when generating numerical solutions. Most parameter values are retrieved from [3]; original sources are listed in the fourth column. Asterisks indicate a dimensionless parameter. Given the model’s representation of village-forest patch geography and focus on *P. vivax* dynamics, parameter values are derived for Southeast Asia and the Americas.

2.4.1 Population-level densities of infectious moving and non-moving individuals

Since the non-moving population is homogeneous with respect to hypnozoite and infection dynamics and the number of non-moving humans is assumed to be arbitrarily large, the density of $I_N(t)$ approaches the product of N and the probability that a single non-moving individual is infectious (see, e.g., the hybrid modeling strategies in [25, 30]). This probability is given by (12) and hence $I_N(t)$ is equal to

$$I_N(t) = N - N \exp \left(\int_0^t \lambda_1(\tau) f(t - \tau) d\tau \right).$$

Similarly, we can closely approximate the density of infectious moving individuals in the population by the expected size of $I_M(t)$. To calculate $I_M(t)$, we let there be a bijection

mapping each moving person $j \in \mathcal{M}$ to a periodic, deterministic *movement function* $\mathcal{B}_j(t)$, equal to 1 if the corresponding individual is on Patch 1 and to 0 otherwise. We note that the probability of an individual with movement function $\mathcal{B}_j(t)$ to be in I_M at time t is, by (13) in Section 2.2,

$$p_j(t) = 1 - \exp \left(\int_0^t \left(\underbrace{\mathcal{B}_j(\tau)}_{\text{Patch 1 indicator function}} \underbrace{\lambda_1(\tau)}_{\text{Patch 1 FORI}} + \underbrace{(1 - \mathcal{B}_j(\tau))}_{\text{Patch 2 indicator function}} \underbrace{\lambda_2(\tau)}_{\text{Patch 2 FORI}} \right) f(t - \tau) d\tau \right).$$

Given $i \in \mathcal{M}$, we assume that, for all $j \in \mathcal{M}$,

$$\mathcal{B}_j(t) = \mathcal{B}_i(t + \tau_j) \tag{16}$$

for some $|\tau_j| \ll 1 \in \mathbb{R}$ and all $t \in [0, \infty)$, i.e., all movement functions coincide up to arbitrarily-small time-shifts. For simplicity and ease of analysis, we will replace each $\mathcal{B}_j(t)$ with its first-order approximation – i.e., the first two terms in the Fourier series for $\mathcal{B}_j(t)$.

Lemma 2.1. *The first-order approximation $B_j(t)$ of $\mathcal{B}_j(t)$ satisfies*

$$\lim_{\sum_{k \in \mathcal{M}} |\tau_k| \rightarrow 0} B_j(t) = u + v \cos(\omega t),$$

where u, v, ω are defined in (5).

Given Lemma 2.1, we can make the approximation

$$\mathcal{B}_j(t) \approx B_j(t) := u + v \cos(\omega t),$$

from where it follows that

$$I_M(t) \approx M - M \exp \left(\int_0^t (A_1(\tau)\lambda_1(\tau) + A_2(\tau)\lambda_2(\tau)) f(t - \tau) d\tau \right). \tag{17}$$

For completeness, we also formulate expressions for $L_N(t)$ and $L_M(t)$. Via a similar argument to the above, we obtain that the density of liver-infected non-moving individuals in the population is

$$L_N(t) = \underbrace{N \exp \left(\int_0^t \lambda_1(t) f(t - \tau) d\tau \right)}_{\text{density of non-moving individuals without blood infections}} - \underbrace{N \exp \left(\int_0^t \lambda_1(t) g(t - \tau) d\tau \right)}_{\text{density of non-moving individuals without liver or blood infections}}, \tag{18}$$

and the density of liver-infected moving individuals is

$$\begin{aligned}
L_M(t) \approx M \exp & \left(\underbrace{\int_0^t \left(\underbrace{A_1(\tau) \lambda_1(\tau)}_{\text{Patch 1 density}} + \underbrace{A_2(\tau) \lambda_2(\tau)}_{\text{Patch 2 density}} \right) f(t - \tau) d\tau}_{\text{density of moving individuals without blood infections}} \right) - \\
& \underbrace{M \exp \left(\int_0^t \left(\underbrace{A_1(\tau) \lambda_1(\tau)}_{\text{Patch 1 density}} + \underbrace{A_2(\tau) \lambda_2(\tau)}_{\text{Patch 2 density}} \right) g(t - \tau) d\tau \right)}_{\text{density of moving individuals without liver or blood infections}}. \tag{19}
\end{aligned}$$

Proof of Lemma 2.1. We first note that the density of individuals on Patch 1 can be written as

$$A_1(t) = \frac{1}{M} \int_j \mathcal{B}_j(t) dj.$$

Since all \mathcal{B}_j have the same period, $\mathcal{B}_j(t) = \mathcal{B}_j(t + 2\pi/\omega)$ for all $j \in M$. Fixing $j \in \mathcal{M}$, we compute that the constant term of the Fourier series for \mathcal{B}_j is

$$\frac{\omega}{2\pi} \int_0^{2\pi/\omega} \mathcal{B}_j(\tau) d\tau = \frac{1}{M} \int_j \left(\frac{\omega}{2\pi} \int_0^{2\pi/\omega} \mathcal{B}_j(\tau) d\tau \right) dj = \frac{\omega}{2\pi} \int_0^{2\pi/\omega} A_1(\tau) d\tau = u. \tag{20}$$

Similarly, upon decomposing all \mathcal{B}_j into Fourier series, we note that, by (16), the second terms of all such Fourier series must be of the form $x \cos(\omega t + \tau_j) + y \sin(\omega t + \tau_j)$. Moreover, $\lim_{\tau_j \rightarrow 0} x = v, \lim_{\tau_j \rightarrow 0} y = 0$ since $\frac{1}{M} \int_j x \cos(\omega t + \tau_j) + y \sin(\omega t + \tau_j) dj = v \cos(\omega t)$. The statement of the lemma follows. \square

2.4.2 Derivation of population-level model with coupled human-mosquito dynamics

To represent mosquito dynamics on both patches, we construct a nonlinear SEI-type model based on [3]. We divide the sets Q_1, Q_2 into three sub-populations each, denoted by S_{mi}, E_{mi}, I_{mi} , $i \in 1, 2$, and representing susceptible, exposed, and infectious mosquitoes, respectively (Figure 4). Here g_i denotes the (constant as opposed to seasonal) birth and death rates for mosquitoes on Patch i , with $g_1 > g_2$. Mosquito sporogony occurs at rate n . The force of infection $\Phi_i(t)$ for mosquitoes on Patch i , $i \in 1, 2$, is the product of the mean mosquito bite rate, a , the probability of human-to-mosquito transmission, c , and the proportion of infectious humans on Patch i (relative to the total number of humans on Patch i). In particular,

$$\begin{aligned}
\Phi_1(t) &= \frac{ac (I_N + (u - v \cos \omega t) I_M)}{N + (u + v \cos \omega t) M}; \\
\Phi_2(t) &= \frac{ac I_M}{M}. \tag{21}
\end{aligned}$$

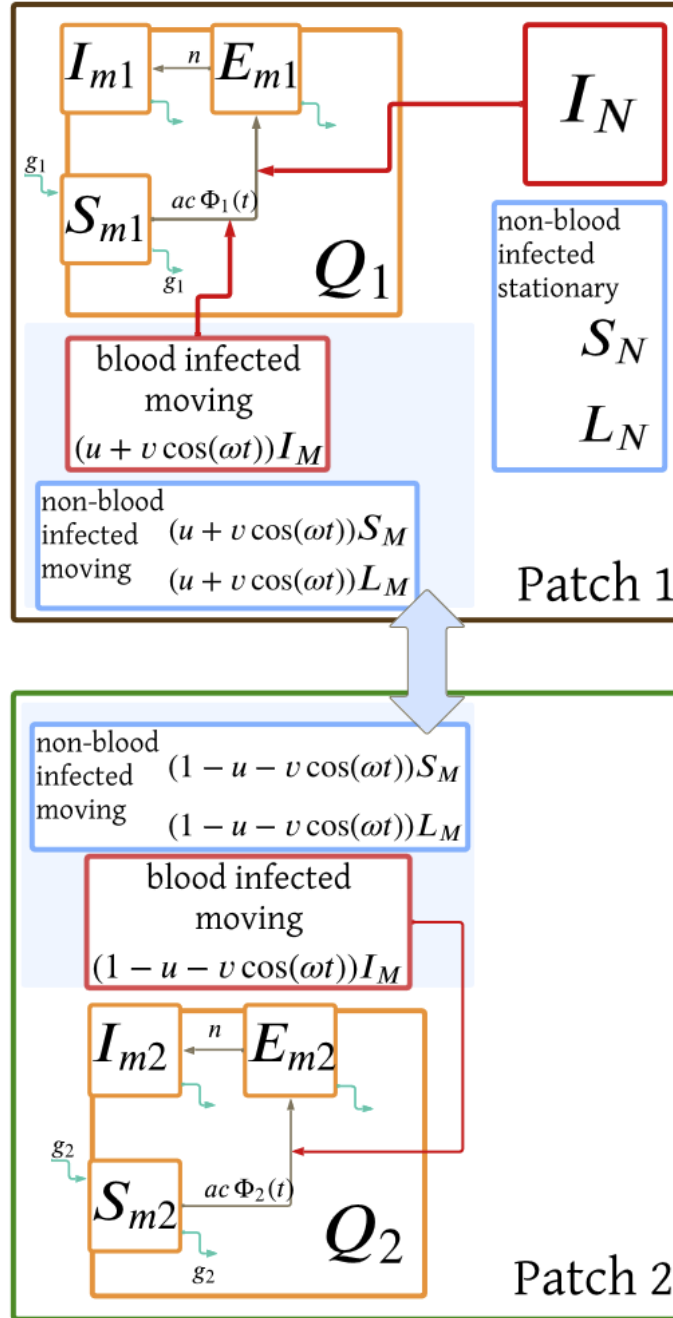


Figure 4: Schematic of the two-patch population-level model. Within-host processes (including recovery, primary infection, or hypnozoite activation mechanisms) is omitted to best display population-level dynamics. The red arrows indicate infection mechanisms, while the large blue arrow represents the migration of moving individuals between Patch 1 (the upper large square) and Patch 2 (the lower large square). Within each patch, the group of moving individuals (including blood-infected, liver-infected, and susceptible travelers) is indicated with a lightly-shaded blue rectangle.

To determine $I_{m1}(t)$ and $I_{m2}(t)$ – functions which then allow us to describe the infection and hypnozoite dynamics of the entire moving and non-moving population – we solely require knowledge of the density of infected non-moving humans, $I_N(t)$, and the density of infected moving humans, $I_M(t)$. As a result, to complete our “minimal” population-level model, we only need equations for $I_N(t)$ and $I_M(t)$. These equations follow directly from Section 2.4.1. Our population-level model can thus be described by the following system of differential equations (with embedded Volterra convolution equations of the first kind):

$$\begin{aligned}
\frac{dS_{m1}}{dt} &= g_1 Q_1 - \frac{ac (I_N + (u + v \cos \omega t) I_M)}{N + (u + v \cos \omega t) M} S_{m1} - g_1 S_{m1}; \\
\frac{dE_{m1}}{dt} &= \frac{ac (I_N + (u + v \cos \omega t) I_M)}{N + (u + v \cos \omega t) M} S_{m1} - (g_1 + n) E_{m1}; \\
\frac{dI_{m1}}{dt} &= n E_{m1} - g_1 I_{m1}; \\
\frac{dS_{m2}}{dt} &= g_2 Q_2 - \frac{ac I_M}{M} S_{m2} - g_2 S_{m2}; \\
\frac{dE_{m2}}{dt} &= \frac{ac I_M}{M} S_{m2} - (g_2 + n) E_{m2}; \\
\frac{dI_{m2}}{dt} &= n E_{m2} - g_2 I_{m2}; \\
I_M &= M - M \exp \left(ab \int_0^t \left(\frac{I_{m1}(\tau)(u + v \cos \omega \tau)}{N + (u + v \cos \omega \tau) M} + \frac{I_{m2}(\tau)((1 - u) - v \cos \omega \tau)}{((1 - u) - v \cos \omega \tau) M} \right) f(t - \tau) d\tau \right); \\
I_N &= N - N \exp \left(ab \int_0^t \frac{I_{m1}(\tau)}{N + (u + v \cos \omega \tau) M} f(t - \tau) d\tau \right)
\end{aligned} \tag{22}$$

with initial conditions

$$\begin{aligned}
S_{m1}(0) &= S_{m1}^{(0)}; E_{m1}(0) = E_{m1}^{(0)}; I_{m1}(0) = I_{m1}^{(0)}; \\
S_{m2}(0) &= S_{m2}^{(0)}; E_{m2}(0) = E_{m2}^{(0)}; I_{m2}(0) = I_{m2}^{(0)}; I_M(0) = 0; I_N(0) = 0.
\end{aligned} \tag{23}$$

We note that this minimal model system does not incorporate the equation for the densities of individuals with liver-only infections. As described above, the solutions for $L_N(t), L_M(t)$ (unlike those for $I_N(t), I_M(t)$) do not directly determine the distribution of mosquitoes across compartments in the population-level model. Moreover, the equations for $L_N(t), L_M(t)$ are uncoupled from those for $I_N(t), I_M(t)$ via the analysis in Section 2.2, meaning that (18) and (19) can be excluded from the model in (22). We return to the implications of the solutions for $I_{m1}(t), I_{m2}(t)$ on $L_N(t), L_M(t)$ in the sections that follow.

2.4.3 Limiting prevalence assuming constant forces of re-infection

We now consider a situation in which the forces of re-infection (FORIs) on patches 1 and 2 – λ_1, λ_2 , respectively – are *constant*. In this case, a single equation may be derived for I_M , which will yield insight for the impact of movement on transmission.

As before, we let the expected proportion of people on patches 1 and 2 at time t be of the form $u + v \cos(\omega t), 1 - u - v \cos(\omega t)$, respectively.

From (17), the density of infectious moving individuals is

$$I_M(t) \approx M - M \exp \left(\lambda_1 \int_0^t (u + v \cos(\omega t)) f(t - \tau) d\tau + \lambda_2 \int_0^t (1 - u - v \cos(\omega t)) f(t - \tau) d\tau \right). \quad (24)$$

We define $I_M^*(t)$ as the periodic function satisfying $\lim_{t \rightarrow \infty} |I_M(t) - I_M^*(t)| = 0$. We seek $I_M^*(t)$ in terms of the parameters, including u, v , and ω . We note that

$$I_M(t) = M - M \exp \left((\lambda_1 u + \lambda_2 (1 - u)) \int_0^t f(\tau) d\tau \right) \exp \left((v\lambda_1 - v\lambda_2) \int_0^t \cos(\omega t) f(t - \tau) d\tau \right), \quad (25)$$

where

$$\int_0^t \cos(\omega \tau) f(t - \tau) d\tau = \frac{1}{2} e^{\omega i t} \int_0^t (e^{-\omega i \tau}) f(\tau) d\tau + \frac{1}{2} e^{-\omega i t} \int_0^t (e^{\omega i \tau}) f(\tau) d\tau. \quad (26)$$

We observe that $I_M^*(t)$ is a periodic function with period $\frac{2\pi}{\omega}$. This follows from the bound

$$\lim_{t \rightarrow \infty} \int_0^t \frac{-e^{-\gamma \tau} - \nu p_A(\tau)}{1 + \nu p_A \left(\frac{\ln(\gamma/(\alpha + \mu))}{-\alpha - \mu + \gamma} \right)} d\tau > \lim_{t \rightarrow \infty} \int_0^t f(\tau) d\tau > \lim_{t \rightarrow \infty} \int_0^t (-e^{-\gamma \tau} - \nu p_A(\tau)) d\tau$$

which implies that the improper integrals

$$C_0 = \lim_{t \rightarrow \infty} \int_0^t f(\tau) d\tau; \quad C_1 := \lim_{t \rightarrow \infty} \int_0^t e^{-\omega i \tau} f(\tau) d\tau; \quad C_{-1} := \lim_{t \rightarrow \infty} \int_0^t e^{\omega i \tau} f(\tau) d\tau, \quad (27)$$

converge to constants in \mathbb{C} .

Fixing $t \gg 1$, from (68), we see that $I_M^*(t)$ is a monotonically-decreasing function of u (where we use the fact that $\lambda_1 < \lambda_2$). Moreover, since $\max_t I_M^*(t) - \min_t I_M^*(t)$ is proportional to the value of

$$\exp(v\lambda_1 - v\lambda_2) \left(\max_t \exp \left(\int_0^t \cos(\omega t) f(t - \tau) d\tau \right) - \min_t \exp \left(\int_0^t \cos(\omega t) f(t - \tau) d\tau \right) \right),$$

$\max_t I_M^*(t) - \min_t I_M^*(t)$ is a monotonically-decreasing function of $|v|$ and a monotonically-increasing function of ω (an equivalent statement will be shown for the non-constant FORI system (22) in Appendix A).

For sufficiently-large ω and sufficiently-small $|v|$, we observe that $I_M(t)$ can be closely decomposed by a constant term and two oscillating terms with frequency $1/\omega$. This is relevant to our choice of ansatz when seeking solutions for the full population-level model with coupled human-vector dynamics.

2.5 Numerical solution of multiscale model

In order to simulate the model in (22), we implemented a solver for integro-differential equations with step size t_{step} (see Algorithm 1). For each value of $t \in k \cdot t_{\text{step}}, k \in \mathbb{Z}, k \in [0, 5000/t_{\text{step}}]$, the solver generated values for $I_M(t)$ and $I_N(t)$ using the history of the FORI. The solver then used the newest values for $I_M(t)$ and $I_N(t)$ to update the values of $S_{m1}, S_{m2}, E_{m1}, E_{m2}, I_{m1}, I_{m2}$ via the fourth-order Runge Kutta. The initial conditions used were $S_{m1} = 0.116, S_{m2} = 0.406, E_{m2} = 0.058, I_{m2} = E_{m1} = I_{m1} = I_N = I_M = 0$.

Algorithm 1

1. Set $t = 0$ and define values for $t_{\text{end}}, t_{\text{step}}$
 2. **while** $t < t_{\text{end}}$ **do**
 - Compute $I_N(t), I_M(t)$ using a Darboux sum with $I_{m1}(\tau), I_{m2}(\tau), \tau \in [0, t]$
 - Update $S_{mi}(t+t_{\text{step}}), E_{mi}(t+t_{\text{step}}), I_{mi}(t+t_{\text{step}}), i \in 1, 2$ using $I_N(t), I_M(t)$ and fourth-order Runge-Kutta (1000 steps) on the time interval $(t, t + t_{\text{step}})$
 - Set $t = t + t_{\text{step}}$
-

3 Results

3.1 Existence and location of the limiting-state solutions of System (22)

Given non-zero v , the system (22) of integro-differential equations is non-autonomous. Setting the left hand sides of the system to zero indicates that (22) possesses only one equilibrium solution, namely the disease-free equilibrium (DFE), satisfying $E_{m1} = E_{m2} = I_{m1} = I_{m2} = I_M = I_N = 0, S_{m1} = Q_1, S_{m2} = Q_2$. Moreover, one can observe from the right hand sides of the equations in (22) that the DFE is the only fixed-point limit set associated to an orbit of the dynamical system defined by (22).

Numerical experiments (see Section 3.2) indicate that the endemic solutions to (22) are asymptotically non-constant periodic, which is further supported by our analysis in the case when the FORI is constant (see Section 2.4.3). In this section, we make the assumption that the biologically-realistic solutions to (22) are limit-periodic, and analyze the location of endemic solutions when they exist.

Accordingly, we seek solutions to (22) that can be decomposed as

$$\begin{aligned}
S_{mi}(t) &= \sum_{n=-\infty}^{\infty} u_n^{(i)}(t) \exp(\omega \mathbf{i} n t), \quad i \in \{1, 2\}; \\
E_{mi}(t) &= \sum_{n=-\infty}^{\infty} v_n^{(i)}(t) \exp(\omega \mathbf{i} n t), \quad i \in \{1, 2\}; \\
I_{mi}(t) &= \sum_{n=-\infty}^{\infty} w_n^{(i)}(t) \exp(\omega \mathbf{i} n t), \quad i \in \{1, 2\}; \\
I_M(t) &= \sum_{n=-\infty}^{\infty} x_n(t) \exp(\omega \mathbf{i} n t); \\
I_N(t) &= \sum_{n=-\infty}^{\infty} y_n(t) \exp(\omega \mathbf{i} n t),
\end{aligned} \tag{28}$$

for complex-valued functions $u_n^{(1)}(t), v_n^{(1)}(t), w_n^{(1)}(t), u_n^{(2)}(t), v_n^{(2)}(t), w_n^{(2)}(t), x_n(t), y_n(t)$ that tend towards a steady state, such that

$$\begin{aligned}
\lim_{t \rightarrow \infty} (u_n^{(1)}(t), v_n^{(1)}(t), w_n^{(1)}(t), u_n^{(2)}(t), v_n^{(2)}(t), w_n^{(2)}(t), x_n(t), y_n(t)) = \\
(u_n^{(1)}, v_n^{(1)}, w_n^{(1)}, u_n^{(2)}, v_n^{(2)}, w_n^{(2)}, x_n, y_n) \in \mathbb{C}^5.
\end{aligned} \tag{29}$$

As $t \rightarrow \infty$, the solutions of (22) can then be described by a Fourier series with constant coefficients. For sufficiently small a, b, c , the right hand sides of (22) imply that the nonconstant arguments of each of our eight limiting solutions are small.

Defining $S_{m1}^*(t)$ as the periodic function satisfying $\lim_{t \rightarrow \infty} (S_{m1}^*(t) - S_{m1}(t)) = 0$, and defining the functions $E_{m1}^*, I_{m1}^*, S_{m2}^*, E_{m2}^*, I_{m2}^*, I_M^*, I_N^*$ similarly, we formulate the ansatz that

$$\begin{aligned}
S_{mi}^*(t) &\approx u_{-1}^{(i)} \exp(-\omega \mathbf{i} t) + u_0^{(i)} + u_1^{(i)} \exp(\omega \mathbf{i} t) + u_\epsilon^{(i)}, \quad i \in \{1, 2\}; \\
E_{mi}^*(t) &\approx v_{-1}^{(i)} \exp(-\omega \mathbf{i} t) + v_0^{(i)} + v_1^{(i)} \exp(\omega \mathbf{i} t) + v_\epsilon^{(i)}, \quad i \in \{1, 2\}; \\
I_{mi}^*(t) &\approx w_{-1}^{(i)} \exp(-\omega \mathbf{i} t) + w_0^{(i)} + w_1^{(i)} \exp(\omega \mathbf{i} t) + w_\epsilon^{(i)}, \quad i \in \{1, 2\}; \\
I_M^*(t) &\approx x_{-1} \exp(-\omega \mathbf{i} t) + x_0 + x_1 \exp(\omega \mathbf{i} t) + x_\epsilon; \\
I_N^*(t) &\approx y_{-1} \exp(-\omega \mathbf{i} t) + y_0 + y_1 \exp(\omega \mathbf{i} t) + y_\epsilon,
\end{aligned} \tag{30}$$

where the Fourier coefficients associated to non-constant terms are much smaller than those associated to constant terms and

$$f_\epsilon^{(i)} \ll f_1^{(i)}, \quad f'_\epsilon \ll f'_1 \tag{31}$$

for $f \in \{u, v, w\}, f' \in \{x, y\}, i \in \{1, 2\}$. We note that the DFE ($u_0^{(1)} = Q_1, u_0^{(2)} = Q_2$, all other coefficients equal to zero) is a solution of (22).

In Appendix A, we find a single nonlinear equation (38), the solution set of which contains all solutions for $w_0^{(2)}$ assuming sufficiently-small $|v|$ and sufficiently-large ω . We also outline a method to extract approximations for all other Fourier coefficients in (30). This yields approximations for the endemic solutions of our system (22) given the ansatz in (30).

To calculate limiting solutions for $L_N(t)$ and $L_M(t)$ from the approximated solutions for $I_{m1}^*(t), I_{m2}^*(t)$, we note that, by (18) and (19),

$$L_N(t) \approx N \exp\left[R(f(t), I_{m1})\right] - N \exp\left[R(g(t), I_{m1})\right], \quad (32)$$

and

$$L_M(t) \approx M \exp\left[R(f(t), I_{m1}) + R(f(t), I_{m2})\right] - M \exp\left[R(g(t), I_{m1}) + R(g(t), I_{m2})\right]. \quad (33)$$

Here,

$$\begin{aligned} R(r(t), I_{m1}) &= \frac{uab \left(\left(\int_0^\infty r(\tau) d\tau \right) w_0^{(1)} + \left(\int_0^\infty e^{-\omega i \tau} r(\tau) d\tau \right) w_1^{(1)} e^{\omega i t} + \left(\int_0^\infty e^{\omega i \tau} r(\tau) d\tau \right) w_{-1}^{(1)} e^{-\omega i t} \right)}{N + Mu} \\ R(r(t), I_{m2}) &= \frac{ab \left(\left(\int_0^\infty r(\tau) d\tau \right) w_0^{(2)} + \left(\int_0^\infty e^{-\omega i \tau} r(\tau) d\tau \right) w_1^{(2)} e^{\omega i t} + \left(\int_0^\infty e^{\omega i \tau} r(\tau) d\tau \right) w_{-1}^{(2)} e^{-\omega i t} \right)}{M}. \end{aligned} \quad (34)$$

The solution set of (38) includes the solution $w_0^{(2)} = 0$ (which implies that all other Fourier coefficients but $u_0^{(1)}, u_0^{(2)}$ are zero, and immediately corresponds to the DFE solution of (22)). In Appendix B, we find necessary and sufficient conditions for (38) to have no endemic solutions. In particular, we obtain the necessary condition

$$\frac{Mg_2(g_2 + n)}{a^2bcn |C_0| Q_2} > 1. \quad (35)$$

and the sufficient condition

$$\frac{Mg_2(g_2 + n)}{Q_2} \left(\frac{1}{a^2bcn |C_0|} - \frac{Q_1Mu}{2g_1(g_1 + n)(N + Mu)} \left(\frac{u + v}{N + (u + v)M} + \frac{u - v}{N + (u - v)M} \right) \right) > 1. \quad (36)$$

We remark on the biological implications of these conditions below.

Remark 3.1. *If*

$$\frac{1}{a^2bcn |C_0|} < \frac{Q_1Mu}{2g_1(g_1 + n)(N + Mu)} \left(\frac{u + v}{N + (u + v)M} + \frac{u - v}{N + (u - v)M} \right),$$

a malaria epidemic may persist indefinitely solely as a result of the Patch 1 mosquito population. Otherwise, the left hand side of (36) is a monotonically-increasing function of $g_1, g_2, |v|$ and a monotonically-decreasing function of $a, b, c, |v|, Q_1, Q_2$. We notice that, for realistic values of parameters such as those in [5], increases in g_1 or decreases in Q_1 may be insufficient to prevent disease endemicity, as

$$Mg_2(g_2 + n) < a^2bcn |C_0| Q_2.$$

However, for sufficiently-large g_2 or sufficiently-small Q_2 , our approximation for (22) has no endemic solutions.

The conditions (35) and (36) suggest that the R_0 for our system satisfies

$$\frac{a^2bcn|C_0|Q_2}{Mg_2(g_2+n)} \leq R_0 \leq \frac{Q_2}{Mg_2(g_2+n) \left(\frac{1}{a^2bcn|C_0|} - \frac{Q_1Mu}{2g_1(g_1+n)(N+Mu)} \left(\frac{u+v}{N+(u+v)M} + \frac{u-v}{N+(u-v)M} \right) \right)}. \quad (37)$$

Remark 3.2. *The lower bound on the R_0 in (37) is equivalent to the basic reproduction number on Patch 2 in the case that the forest patch contains a non-moving population of density M (such that the movement between the patches is removed). In other words, if the system does not approach the DFE in a homogeneous population of density M , (38) possesses endemic solutions.*

We prove Theorem 4.2 in Appendix B. The claim in Remark 3.2 is addressed in Appendix C.

3.2 Numerical results

Solutions for $I_N(t)$, $I_M(t)$, $I_{m1}(t)$, $I_{m2}(t)$ from (22) for parameter values implying slower movement shows peaks in $I_M(t)$ and $I_{m1}(t)$ are closely aligned with troughs in $I_N(t)$ and $I_{m2}(t)$, respectively; oscillations are small and difficult to discern (Figure 5). We note that even low-to-moderate proportions of infectious mosquitoes (e.g., 8% of all mosquitoes on Patch 1, 19% of all mosquitoes on Patch 2) can result in very high densities of blood-infected moving individuals: the proportion of infectious moving humans relative to the total human population is approximately 0.3939, meaning that approximately 98% of \mathcal{M} is infectious for the parameter values in Table 1, in comparison to approximately 17% of \mathcal{N} .

Though the mean period of human movement does not significantly impact the density of infectious individuals, longer periods of movement correspond to greater fluctuations in non-moving human prevalence (Figure 6). As described analytically in Appendix A, the amplitude of oscillations in solutions to (22) is a monotonically decreasing function of ω . As a result, if the periodic forcing associated with migration is seasonal, movement patterns may have a significant impact on prevalence at any given time.

For both $\omega = 1 \text{ day}^{-1}$ and $\omega = 1/120 \text{ day}^{-1}$, the density of blood-infected individuals is far higher in M than in N , owing to the difference in FORI experienced by the two subpopulations (Figure 6). Liver infectiousness in N peaks early and recedes as $t \rightarrow \infty$; liver infectiousness in M and blood infectiousness in both groups is monotonically increasing.

We calculated approximate solutions for (22) under the parameter values in Table 1 by first obtaining the largest solution of (38), at which point the value of $w_0^{(2)}$ was used to find all remaining Fourier coefficients in (30). Analytical approximations generally correspond to numerical solutions (Figure 7). We note that the approximate solutions for $I_M^*(t)$ and $I_{m2}^*(t)$ are particularly close to the numerical ones (less than 0.015% lower), while the approximated solutions for $I_N^*(t)$ and $I_{m1}^*(t)$ are less accurate (up to 3% lower). Figure 8, however, illustrates that the approximation for I_N^* grows closer to the numerical solution as v decreases and u increases.

Comparing the constant-FORI expression for $I_M^*(t)$ in 2.4.3 to the numerical solution for $I_M^*(t)$ in (22) implies that variation in mosquito prevalence (here generated by human movement) propels and reinforces disease transmission across patches (Figure 9). In particular,

numerical solutions to (22) for $I_M(t), t \gg 1$, were compared with solutions to (25) (generated by setting the constant proportion of infectious mosquitoes on Patch 1 to $I_{m1}^c = 0.008$, slightly above the maximum of the solution for $I_{m1}^*(t)$ in (22), and by setting the constant proportion of infectious mosquitoes on Patch 2 to $I_{m2}^c = 0.089$, above the solution for $I_{m2}^*(t)$ in (22)). This choice of constant FORI ensured that

$$I_{m1}^c, I_{m2}^c(t) > I_{m1}(\tau), I_{m2}(\tau)$$

for all τ , i.e., that the proportion of infectious mosquitoes in the constant-FORI case exceeded that in the non-constant-FORI case for all times. Nonetheless, the constant-FORI solution for $I_M^*(t)$ proved significantly smaller than the non-constant FORI solution. This implies that the oscillations in mosquito prevalence, and by extension migration patterns, must be a cause for the extremely high prevalence in Figure 5.

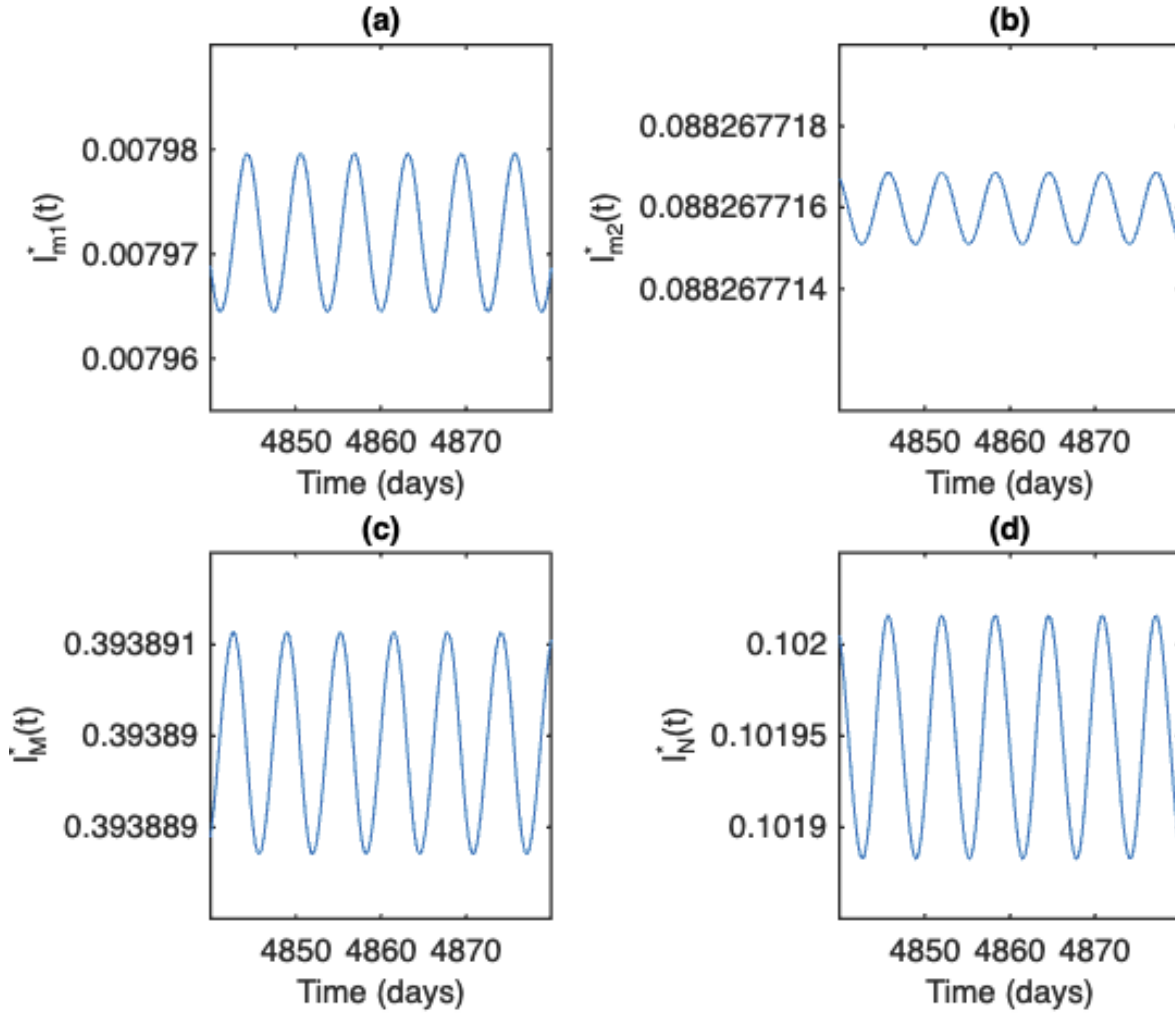
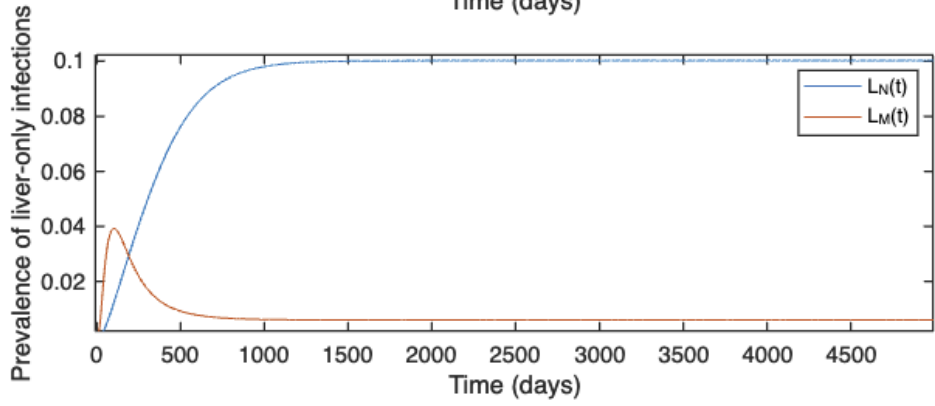
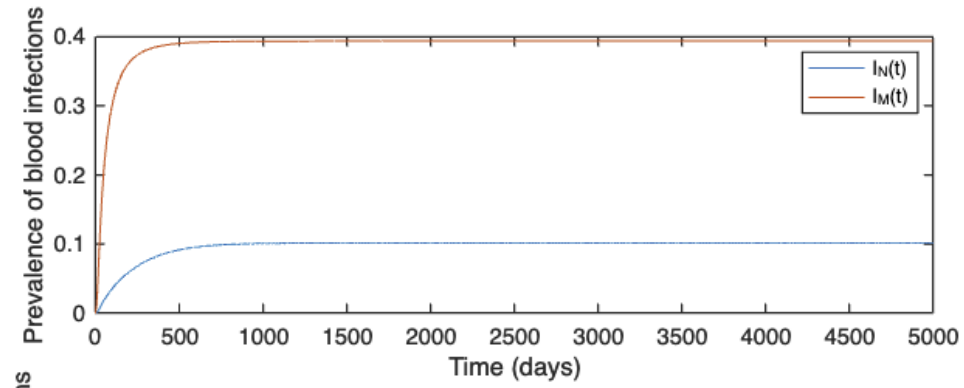
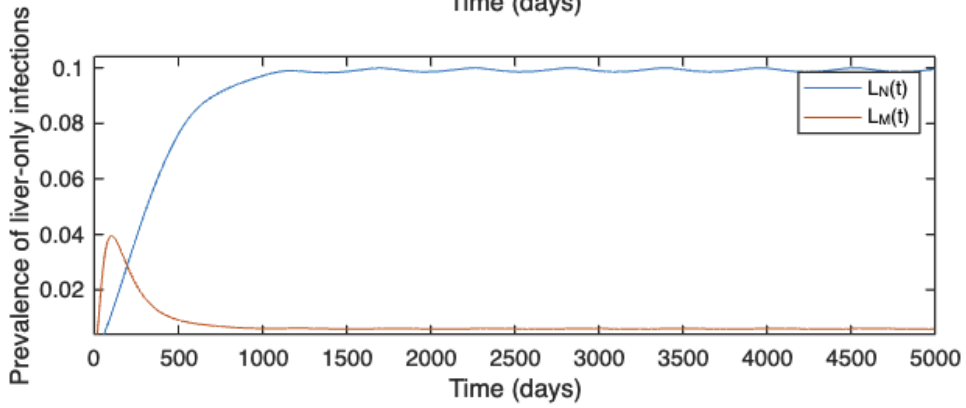
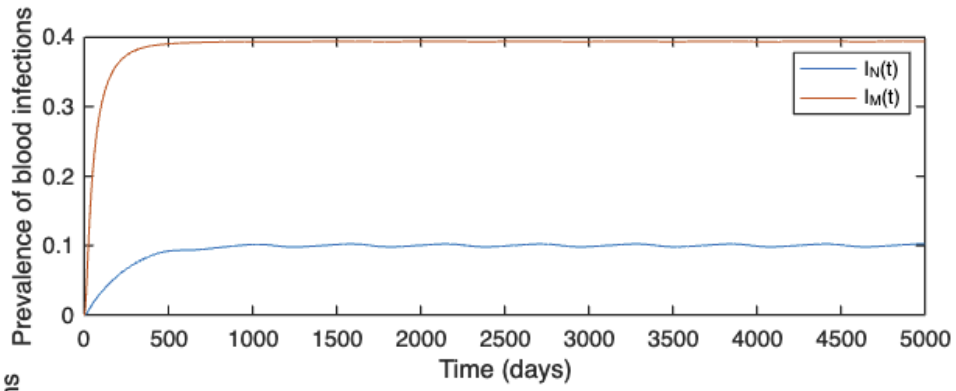


Figure 5: Solutions to (22) using parameter values found in Table 1, with the exception of ω , which was set to $1/5 \text{ days}^{-1}$. Asterisks denote solution asymptotics.



(a)



(b)

Figure 6: Prevalence of blood and liver infections for (a) $\omega = 1 \text{ day}^{-1}$ and (b) $\omega = 1/120 \text{ days}^{-1}$. Numerical solutions were computed using (22).

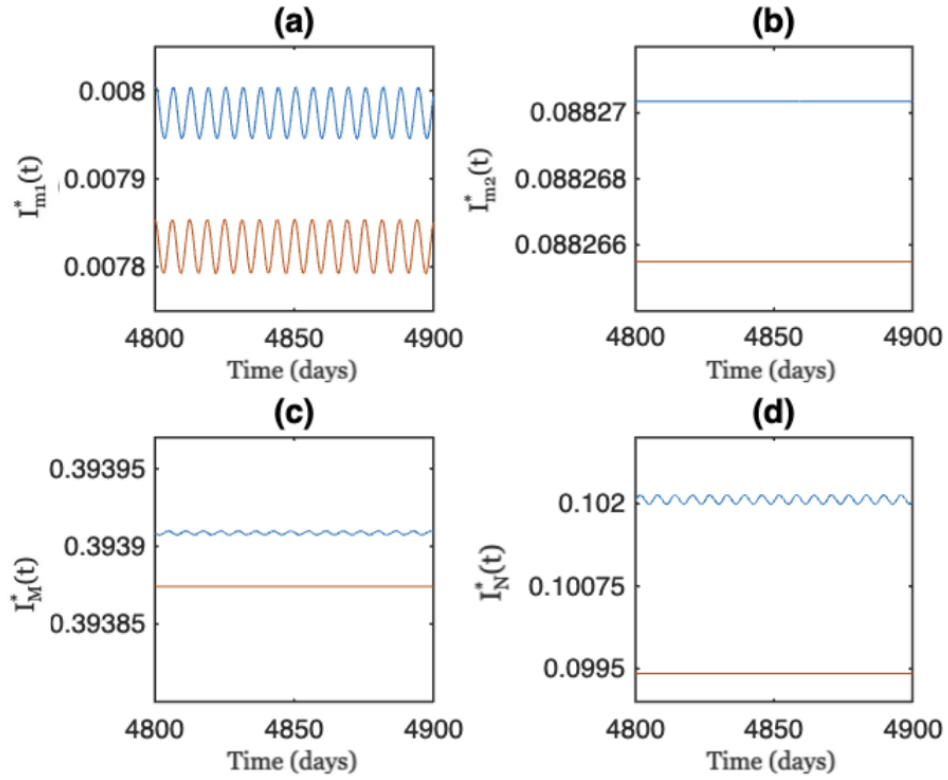
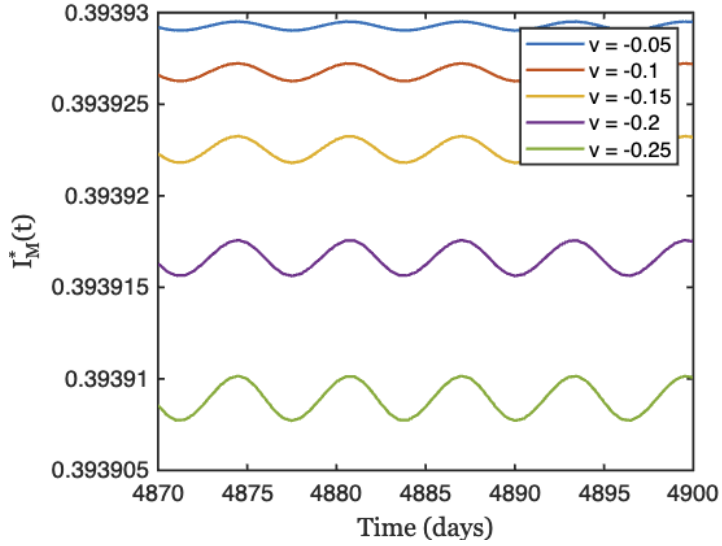


Figure 7: Approximate solutions of (38) are compared to numerical solutions of (22) for each of (a) $I_{m2}^*(t)$, (b) $I_{m1}^*(t)$, (c) $I_M^*(t)$, and (d) $I_N^*(t)$, using the parameter values in Table 1. In each plot, the blue curve illustrates the numerical solution, while the orange curve illustrates the approximate solution, derived by retrieving the largest solution of (38).



(a)



(b)

Figure 8: (a) Percent difference between the numerical solution of (22) and the analytical approximation for I_N^* (values inside the heatmap) for various values of u, v . The approximated solution is derived by first finding the largest solution for $w_0^{(2)}$ of (38), and then using (62), (67) in Appendix A to find y_0 . (b) Prevalence among moving individuals after 4870 days for various v . Remaining parameters are fixed at the values in Table 1.

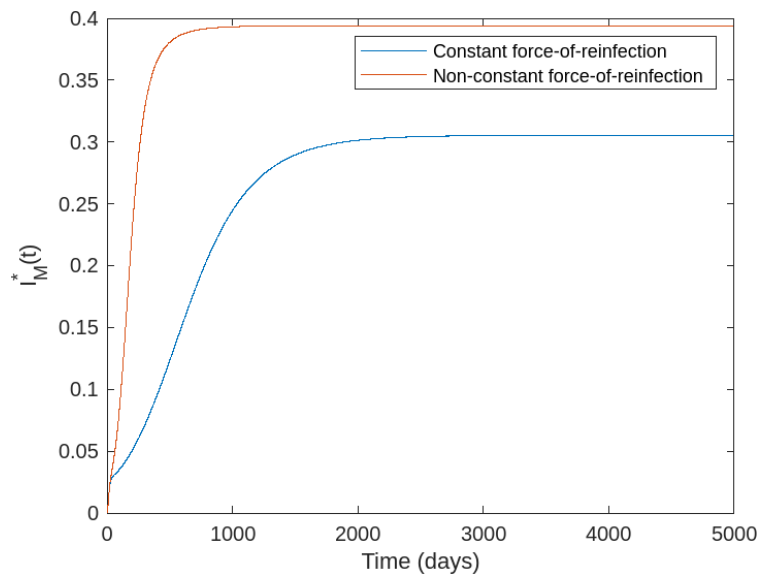


Figure 9: Comparison between limiting-state solution for $I_M(t)$ assuming constant FORI (see (25), blue line) and non-constant FORI (brown line). Parameter values taken from Table 1; values of λ_1, λ_2 for the constant FORI case selected to slightly exceed the limiting prevalence among mosquito populations on Patches 1 and 2, respectively, in the non-constant FORI case.

4 Discussion

In this paper, we use a three-scale mathematical model – combining the within-host, population-based, and spatial levels of analysis – to study the impact of periodic travel patterns on the prevalence of *Plasmodium vivax* infections. Our analysis centers on a two-patch “village-forest” model characterized by the cyclic migration of a subset of humans from the low-transmission “village” patch to the high-transmission “forest” patch. In constructing our model, we further extend the framework developed in [3] and [26].

We circumvent the need to include direct interactions between compartments of susceptible, liver-infected, and blood-infected humans, by recognizing that the distribution across mosquito states depends only on the densities of *infectious* humans, which can in turn be approximated as functions of the infectious mosquito population using PGFs for within-host dynamics. This observation reduces the complexity of our model, allowing us to compose a “minimal” system of IDEs, (22), but also leads us to introduce an additional assumption in Section 2.4.1, where we suppose that all individuals move near-identically. Embedding the within-host framework from [26] into the model ensures that we account for *superinfection*, in which individuals can possess multiple blood-stage infections simultaneously.

In order to study the model system (22), we introduce the ansatz in Section 3.1 that the asymptotic solutions of the system can be closely approximated by rapidly-convergent Fourier series, from where we reduce the original system (22) to a single nonlinear equation, (38), in Appendix A. In Appendix B, we determine necessary and sufficient parameter-based conditions for which the only solution to (38) corresponds to the DFE, obtaining bounds for the system’s basic reproduction number, R_0 (see Section 3.1). Though these results capture the impact of movement on the upper and lower bounds for R_0 , the approximations underlying them are only reasonable for large ω and small v .

To our knowledge, our analysis is the first to incorporate the complex within-host dynamics of hypnozoite inoculation, activation, and clearance characteristic of *P. vivax* into upper and lower bounds for a metapopulation model R_0 . It may also be possible to extend the system asymptotics analysis in Appendix A and the bounds on the R_0 to a larger n -patch case, using certain simplifying assumptions on the inter-patch movement (e.g., assumptions on the extent of coupling between limiting equations in the metapopulation model).

4.1 Biological Insights and Conclusions

Multiple biological applications can be proposed for the model introduced in this paper. Oscillations in malaria prevalence are frequently noted in both human and *Anopheles* populations, but are commonly attributed solely to seasonal fluctuations in mosquito number [18]. Our work suggests that, although the fundamental frequency of these oscillations is likely determined by seasonal changes, higher-frequency harmonics in the prevalence may be induced by the cyclic migration of individuals (which may repeat weekly-to-monthly [5]).

Moreover, though the mean frequency of movement does not impact average *Plasmodium vivax* prevalence, less frequent movement results in greater variation in prevalence over time. We show that individuals traveling between a forest patch with high *Anopheles* density and a village patch with low *Anopheles* density see as much risk – or more – compared to individuals isolated on the forest patch, which emphasizes the role in movement in exacerbating *P. vivax*

epidemics.

The sufficient and necessary conditions for our approximated equations to have no endemic solutions imply interesting results regarding the impact of parameters on the *P. vivax* basic reproduction number. The upper bound on R_0 , for instance, is a strictly decreasing function of $|v|$, meaning that a larger value for $|v|$ — corresponding to more individuals traveling in groups — may enable the system to reach a disease-free equilibrium. Moreover, the lower bound on R_0 have no nonzero solutions is completely independent of g_1 (the village mosquito death rate) and Q_1 (the village mosquito population size), while the upper bound depends far more strongly on g_2, Q_2 (the forest mosquito death rate and population size, respectively) than on g_1, Q_1 . In the case of *P. vivax* in populations of traveling loggers and farmers (so-called “forest goers”) in Southeast Asia, our work stresses the need to control forest mosquito populations in addition to village ones, emphasizing the use of outdoor-acting interventions such as spatial repellents, sterile insect techniques, and source reduction [1, 19, 21, 22].

In future work, we plan to extend these results to the location of endemic solutions, considering the impact of mass drug administration and non-pharmaceutical interventions on *P. vivax* prevalence. We also plan to incorporate correlates of immunity in the model, which may alter the clear \mathcal{M} -dominated patterns of prevalence visible in Section 2.5 above.

Addressing the continued endemicity of malaria in regions across Southeast Asia, the Americas, and the Pacific requires a thorough understanding of each of the mechanisms propelling *P. vivax* transmission, and of the interplay between them. As the first paper consolidating representations of the three major scales – the within-host, population, and metapopulation levels – at which *P. vivax* epidemiological dynamics occur, we have devised a framework in this paper that can be used to predict *P. vivax* prevalence and to establish conditions for disease eradication given a variety of biological and geographical phenomena.

Appendix A: Analytical Approximations for Fourier Coefficients in (30)

We prove the following result:

Theorem 4.1. *For sufficiently-small $|v|$ and sufficiently-large ω , the solution for $w_0^{(2)}$ is contained in the solution set of the nonlinear equation*

$$F_1(w_0^{(2)}, A(w_0^{(2)})) + F_2(w_0^{(2)}, A(w_0^{(2)})) = H(A(w_0^{(2)})), \quad (38)$$

where

$$F_1(w_0^{(2)}, A(w_0^{(2)})) = \frac{N - N \exp\left(\frac{ab|C_0|A(w_0^{(2)})}{N+Mu}\right) + \frac{M(u+v)g_2(g_2+n)w_0^{(2)}}{ac(Q_2n-(g_2+n)w_0^{(2)})}}{N + (u+v)M}$$

$$F_2(w_0^{(2)}, A(w_0^{(2)})) = \frac{N - N \exp\left(\frac{ab|C_0|A(w_0^{(2)})}{N+Mu}\right) + \frac{M(u-v)g_2(g_2+n)w_0^{(2)}}{ac(Q_2n-(g_2+n)w_0^{(2)})}}{N + (u-v)M}, \quad (39)$$

$$H(A(w_0^{(2)})) = \frac{2g_1A(w_0^{(2)})(g_1+n)}{ac\left(nQ_1 - (g_1+n)A(w_0^{(2)})\right)},$$

$$A(w_0^{(2)}) = \frac{N + Mu}{abC_0u} \left(\frac{ab|C_0|w_0^{(2)}}{M} + \ln \left(1 - \frac{g_2(g_2+n)w_0^{(2)}}{ac(Q_2n-(g_2+n)w_0^{(2)})} \right) \right),$$

$$C_0 = \lim_{t \rightarrow \infty} \int_0^t f(\tau) d\tau, \quad (40)$$

and a unique value for all other Fourier coefficients (and hence limiting-state solutions for (22)) can be determined from the value of $w_0^{(2)}$. In particular, when the only solution of (38) is $w_0^{(2)} = 0$, no endemic solution exists. If nonzero solutions of (38) exist, then one can extract periodic endemic solutions approximately corresponding to solutions for (22).

Proof. We first write equations for the Fourier coefficients in (30). The first six equations in (22) can be written as

$$\left(N + M \left(u + \frac{v}{2} e^{\omega it} + \frac{v}{2} e^{-\omega it} \right) \right) \sum_{k=-1}^1 \mathbf{i} j u_j^{(1)} e^{\omega \mathbf{i} j t} =$$

$$\left(N + M \left(u + \frac{v}{2} e^{\omega it} + \frac{v}{2} e^{-\omega it} \right) \right) \left(g_1 Q_1 - g_1 \sum_{j=-1}^1 u_j^{(1)} e^{\omega \mathbf{i} j t} \right) - \quad (41)$$

$$ac \left(\sum_{j=-1}^1 u_j^{(1)} e^{\omega \mathbf{i} j t} \right) \left(\sum_{j=-1}^1 y_j e^{\omega \mathbf{i} j t} + \left(u + \frac{v}{2} e^{\omega it} + \frac{v}{2} e^{-\omega it} \right) \sum_{j=-1}^1 x_j e^{\omega \mathbf{i} j t} \right),$$

$$\left(N + M \left(u + \frac{v}{2} e^{\omega it} + \frac{v}{2} e^{-\omega it} \right) \right) \sum_{j=-1}^1 \mathbf{i} j v_j^{(1)} e^{\omega \mathbf{i} j t} =$$

$$ac \left(\sum_{j=-1}^1 u_j^{(1)} e^{\omega \mathbf{i} j t} \right) \left(\sum_{j=-1}^1 y_j e^{\omega \mathbf{i} j t} + \left(u + \frac{v}{2} e^{\omega it} + \frac{v}{2} e^{-\omega it} \right) \sum_{j=-1}^1 x_j e^{\omega \mathbf{i} j t} \right) - \quad (42)$$

$$(g_1 + n) \left(N + M \left(u + \frac{v}{2} e^{\omega it} + \frac{v}{2} e^{-\omega it} \right) \right) \left(\sum_{j=-1}^1 v_j^{(1)} e^{\omega \mathbf{i} j t} \right),$$

$$\sum_{j=-1}^1 \mathbf{i} j w_j^{(1)} e^{\omega \mathbf{i} j t} = j \sum_{j=-1}^1 v_j^{(1)} e^{\omega \mathbf{i} j t} - g_1 \sum_{j=-1}^1 w_j^{(1)} e^{\omega \mathbf{i} j t}, \quad (43)$$

$$\sum_{j=-1}^1 \mathbf{i} j u_j^{(2)} e^{\omega \mathbf{i} j t} = g_2 Q_2 - \frac{ac}{2M} \left(\sum_{j=-1}^1 u_j^{(2)} e^{\omega \mathbf{i} j t} \right) \left(\sum_{j=-1}^1 x_j e^{\omega \mathbf{i} j t} \right) - g_2 \sum_{j=-1}^1 u_j^{(2)} e^{\omega \mathbf{i} j t}, \quad (44)$$

$$\sum_{j=-1}^1 \mathbf{i} j v_j^{(2)} e^{\omega \mathbf{i} j t} = \frac{ac}{2M} \left(\sum_{j=-1}^1 u_j^{(2)} e^{\omega \mathbf{i} j t} \right) \left(\sum_{j=-1}^1 x_j e^{\omega \mathbf{i} j t} \right) - (g_2 + n) \sum_{j=-1}^1 v_j^{(2)} e^{\omega \mathbf{i} j t}, \quad (45)$$

$$\sum_{j=-1}^1 \mathbf{i} j w_j^{(2)} e^{\omega \mathbf{i} j t} = n \sum_{j=-1}^1 v_j^{(2)} e^{\omega \mathbf{i} j t} - g_2 \sum_{j=-1}^1 w_j^{(2)} e^{\omega \mathbf{i} j t}. \quad (46)$$

To deal with the unwieldy equations (41) through (46), we first make the change of parameters

$$y = y_{-1} + y_0 + y_1; \quad w_1 = w_{-1}^{(1)} + w_0^{(1)} + w_1^{(1)}; \quad w_2 = w_{-1}^{(2)} + w_0^{(2)} + w_1^{(2)}; \quad v_1 = v_{-1}^{(1)} + v_0^{(1)} + v_1^{(1)}; \\ v_2 = v_{-1}^{(2)} + v_0^{(2)} + v_1^{(2)}; \quad u_1 = u_{-1}^{(1)} + u_0^{(1)} + u_1^{(1)}; \quad u_2 = u_{-1}^{(2)} + u_0^{(2)} + u_1^{(2)}; \quad x = x_{-1} + x_0 + x_1, \quad (47)$$

$$y^* = y_0 + \mathbf{i}(y_1 - y_{-1}); \quad w_1^* = w_0^{(1)} + \mathbf{i}(w_1^{(1)} - w_{-1}^{(1)}); \quad w_2^* = w_0^{(2)} + \mathbf{i}(w_1^{(2)} - w_{-1}^{(2)}); \\ v_1^* = v_0^{(1)} + \mathbf{i}(v_1^{(1)} - v_{-1}^{(1)}); \quad v_2^* = v_0^{(2)} + \mathbf{i}(v_1^{(2)} - v_{-1}^{(2)}); \quad u_1^* = u_0^{(1)} + \mathbf{i}(u_1^{(1)} - u_{-1}^{(1)}); \quad (48) \\ u_2^* = u_0^{(2)} + \mathbf{i}(u_1^{(2)} - u_{-1}^{(2)}); \quad x^* = x_0 + \mathbf{i}(x_1 - x_{-1}),$$

and

$$\bar{y} = y_{-1} - y_0 - y_1; \quad \bar{w}_1 = w_{-1}^{(1)} - w_0^{(1)} - w_1^{(1)}; \quad \bar{w}_2 = w_{-1}^{(2)} - w_0^{(2)} - w_1^{(2)}; \quad \bar{v}_1 = v_{-1}^{(1)} - v_0^{(1)} - v_1^{(1)}; \\ \bar{v}_2 = v_{-1}^{(2)} - v_0^{(2)} - v_1^{(2)}; \quad \bar{u}_1 = u_{-1}^{(1)} - u_0^{(1)} - u_1^{(1)}; \quad \bar{u}_2 = u_{-1}^{(2)} - u_0^{(2)} - u_1^{(2)}, \quad \bar{x} = x_{-1} - x_0 - x_1. \quad (49)$$

Given this change of parameters, we can substitute the values $t = 0$, $t = \pi$, and $t = \pi/2$ into (41) through (46) to obtain 24 equations for the 24 new parameters above. We then eliminate $u_1, u_1^*, \bar{u}_1, u_2, u_2^*, \bar{u}_2$ and $v_1, v_1^*, \bar{v}_1, v_2, v_2^*, \bar{v}_2$ by using the relations

$$v_1 = \frac{g_1 w_1}{n} + \frac{2w_1^* - w_1 - \bar{w}_1}{2n} \\ v_1^* = \frac{g_1 w_1^*}{n} - \frac{w_1 - \bar{w}_1}{2n} \\ \bar{v}_1 = \frac{g_1 \bar{w}_1}{n} - \frac{2w_1^* - w_1 - \bar{w}_1}{2n}, \quad (50)$$

and

$$\begin{aligned}
u_1 &= Q_1 - \frac{(g_1 + n)w_1}{n} - \frac{2w_1^* - w_1 - \bar{w}_1}{2n} \\
u_1^* &= Q_1 - \frac{(g_1 + n)w_1^*}{n} + \frac{w_1 - \bar{w}_1}{2n} \\
\bar{u}_1 &= Q_1 - \frac{(g_1 + n)\bar{w}_1}{n} + \frac{2w_1^* - w_1 - \bar{w}_1}{2n}.
\end{aligned} \tag{51}$$

After applying the change of parameters to (41) and (44), we can solve for x, x^*, \bar{x} and y, y^*, \bar{y} in terms of w_2, w_2^*, \bar{w}_2 and w_1, w_1^*, \bar{w}_1 . We can then rewrite the result in terms of the original Fourier series coefficients for $I_{m1}(t), I_{m2}(t)$. In doing so, we obtain

$$\begin{aligned}
x &= \frac{M \left(g_2(g_2 + n)(w_0^{(2)} + w_1^{(2)} + w_{-1}^{(2)}) + (2g_2 + n)(\mathbf{i} \cdot w_1^{(2)} - \mathbf{i} \cdot w_{-1}^{(2)}) - w_1^{(2)} - w_{-1}^{(2)} \right)}{ac \left(nQ_2 - (g_2 + n)(w_0^{(2)} + w_1^{(2)} + w_{-1}^{(2)}) - (\mathbf{i} \cdot w_1^{(1)} - \mathbf{i} \cdot w_{-1}^{(1)}) \right)}, \\
x^* &= \frac{M \left(g_2(g_2 + n)(w_0^{(2)} + (\mathbf{i} \cdot w_1^{(2)} - \mathbf{i} \cdot w_{-1}^{(2)})) - (2g_2 + n)(w_1^{(2)} + w_{-1}^{(2)}) - (\mathbf{i} \cdot w_1^{(2)} - \mathbf{i} \cdot w_{-1}^{(2)}) \right)}{ac \left(nQ_2 - (g_2 + n)(w_0^{(2)} + (\mathbf{i} \cdot w_1^{(2)} - \mathbf{i} \cdot w_{-1}^{(2)})) + w_1^{(2)} + w_{-1}^{(2)} \right)}, \\
\bar{x} &= \frac{M \left(g_2(g_2 + n)(w_0^{(2)} - w_1^{(2)} - w_{-1}^{(2)}) - (2g_2 + n)(\mathbf{i} \cdot w_1^{(1)} - \mathbf{i} \cdot w_{-1}^{(1)}) + w_1^{(1)} + w_{-1}^{(1)} \right)}{ac \left(nQ_2 - (g_2 + n)(w_0^{(2)} - w_1^{(2)} - w_{-1}^{(2)}) + (\mathbf{i} \cdot w_1^{(1)} - \mathbf{i} \cdot w_{-1}^{(1)}) \right)},
\end{aligned} \tag{52}$$

and

$$\begin{aligned}
(y + (u + v)x) &= \left(\frac{N + (u + v)M}{ac} \right) \\
\frac{g_1(g_1 + n)(w_0^{(1)} + w_{-1}^{(1)} + w_1^{(1)}) + (2g_1 + n)(\mathbf{i} \cdot w_1^{(1)} - \mathbf{i} \cdot w_{-1}^{(1)}) - (w_1^{(1)} + w_{-1}^{(1)})}{nQ_1 - (g_1 + n)(w_0^{(1)} + w_{-1}^{(1)} + w_1^{(1)}) - (\mathbf{i} \cdot w_1^{(1)} - \mathbf{i} \cdot w_{-1}^{(1)})}, \\
(y^* + ux^*) &= \left(\frac{N + Mu}{ac} \right) \\
\frac{g_1(g_1 + n)(w_0^{(1)} + \mathbf{i} \cdot w_1^{(1)} - \mathbf{i} \cdot w_{-1}^{(1)}) - (2g_1 + n)(w_1^{(1)} + w_{-1}^{(1)}) - (\mathbf{i} \cdot w_1^{(1)} - \mathbf{i} \cdot w_{-1}^{(1)})}{nQ_1 - (g_1 + n)(w_0^{(1)} + \mathbf{i} \cdot w_1^{(1)} - \mathbf{i} \cdot w_{-1}^{(1)}) + w_1^{(1)} + w_{-1}^{(1)}}, \\
(\bar{y} + (u - v)\bar{x}) &= \left(\frac{N + (u - v)M}{ac} \right) \\
\frac{g_1(g_1 + n)(w_0^{(1)} - w_{-1}^{(1)} - w_1^{(1)}) - (2g_1 + n)(\mathbf{i} \cdot w_1^{(1)} - \mathbf{i} \cdot w_{-1}^{(1)}) + (w_1^{(1)} + w_{-1}^{(1)})}{nQ_1 - (g_1 + n)(w_0^{(1)} - w_{-1}^{(1)} - w_1^{(1)}) + (\mathbf{i} \cdot w_1^{(1)} - \mathbf{i} \cdot w_{-1}^{(1)})}.
\end{aligned} \tag{53}$$

To deal with the remaining two equations in (22), we note that, for sufficiently-small $|v|$ and sufficiently-large ω ,

$$\begin{aligned} \lim_{t \rightarrow \infty} ab \int_0^t \left(\frac{I_{m1}(\tau)}{N + (u + v \cos(\omega\tau)) M} - \frac{I_{m1}(\tau)}{N + Mu} \right) f(t - \tau) d\tau &\approx \\ \frac{w_0^{(1)} ab v M}{N + Mu} \lim_{t \rightarrow \infty} \int_0^t \left(\frac{\cos(\omega\tau)}{N + (u + v \cos(\omega\tau)) M} f(t - \tau) \right) d\tau &\ll 1 \end{aligned} \quad (54)$$

and

$$\begin{aligned} \lim_{t \rightarrow \infty} ab \int_0^t \left(\frac{I_{m1}(\tau) (u + v \cos(\omega\tau))}{N + (u + v \cos(\omega\tau)) M} - \frac{u I_{m1}(\tau)}{N + Mu} \right) f(t - \tau) d\tau &\approx \\ \frac{w_0^{(1)} ab v N}{N + Mu} \lim_{t \rightarrow \infty} \int_0^t \left(\frac{\cos(\omega\tau)}{N + (u + v \cos(\omega\tau)) M} f(t - \tau) \right) d\tau &\ll 1, \end{aligned} \quad (55)$$

as ab is small, $\frac{M}{N+Mu} < 1$, and $w_0^{(1)} < Q_1$ (where Q_1 is assumed to be $\ll 1$).

As such, we can make the zero-order approximation

$$\begin{aligned} \lim_{t \rightarrow \infty} I_M(t) &= M \left(1 - \exp \left(ab \int_0^t \left(\frac{u I_{m1}(\tau)}{N + Mu} + \frac{I_{m2}(\tau)}{M} \right) f(t - \tau) d\tau \right) \right), \\ \lim_{t \rightarrow \infty} I_N(t) &= N \left(1 - \exp \left(ab \int_0^t \frac{I_{m1}(\tau)}{N + Mu} f(t - \tau) d\tau \right) \right). \end{aligned} \quad (56)$$

It follows that

$$\begin{aligned} y_0 + y_{-1} e^{-it} + y_1 e^{it} &\approx N - N \exp \left(\frac{ab C_0 w_0^{(1)} + ab C_1 w_1^{(1)} e^{\omega it} + ab C_{-1} w_{-1}^{(1)} e^{-\omega it}}{N + Mu} \right) \\ &\approx N - N \exp \left(\frac{ab C_0 w_0}{N + Mu} \right) \left(1 + \frac{ab C_1 w_1^{(1)} e^{\omega it} + ab C_{-1} w_{-1}^{(1)} e^{-\omega it}}{N + Mu} \right), \end{aligned} \quad (57)$$

since by our ansatz $w_1^{(1)}, w_{-1}^{(1)} \ll 1$. Similarly,

$$\begin{aligned} x_0 + x_{-1} e^{-\omega it} + x_1 e^{\omega it} &\approx M - M \exp \left(\frac{uab (C_0 w_0^{(1)} + C_1 w_1^{(1)} e^{\omega it} + C_{-1} w_{-1}^{(1)} e^{-\omega it})}{N + Mu} \right) \\ &\quad \times \exp \left(\frac{ab (C_0 w_0^{(2)} + C_1 w_1^{(2)} e^{\omega it} + C_{-1} w_{-1}^{(2)} e^{-\omega it})}{M} \right) \\ &\approx M - M \exp \left(\frac{uab C_0 w_0^{(1)}}{N + uM} \right) \exp \left(\frac{ab C_0 w_0^{(2)}}{M} \right) \\ &\quad \left(1 + \frac{ab C_1 w_1^{(2)} e^{\omega it} + ab C_{-1} w_{-1}^{(2)} e^{-\omega it}}{M} + \frac{uab (C_1 w_1 e^{\omega it} + C_{-1} w_{-1} e^{-\omega it})}{N + Mu} \right). \end{aligned} \quad (58)$$

We note that (57) and (58) imply that the amplitude of I_M^*, I_N^* is a decreasing function of ω . This can be seen by viewing C_1, C_{-1} as functions of ω , i.e., $C_1 = C_1(\omega), C_{-1} = C_{-1}(\omega)$, and noting that $\frac{d}{d\omega} |C_{-1} + C_1|, \frac{d}{d\omega} |C_{-1} - C_1| < 0$.

From (57) and (58), it follows that

$$x_0 \approx M - M \exp\left(\frac{uab C_0 w_0^{(1)}}{N + uM}\right) \exp\left(\frac{ab C_0 w_0^{(2)}}{M}\right), \quad (59)$$

$$x_1 \approx -M \exp\left(\frac{uab C_0 w_0^{(1)}}{N + Mu}\right) \exp\left(\frac{ab C_0 w_0^{(2)}}{M}\right) \left(\frac{ab C_1 w_1^{(2)}}{M} + \frac{uab C_1 w_1^{(1)}}{N + Mu}\right), \quad (60)$$

and

$$x_{-1} \approx -M \exp\left(\frac{uab C_0 w_0^{(1)}}{N + uM}\right) \exp\left(\frac{ab C_0 w_0^{(2)}}{M}\right) \left(\frac{ab C_{-1} w_{-1}^{(2)}}{M} + \frac{uab C_{-1} w_{-1}^{(1)}}{N + Mu}\right), \quad (61)$$

while

$$y_0 \approx N - N \exp\left(\frac{ab C_0 w_0^{(1)}}{N + Mu}\right), \quad (62)$$

$$y_1 \approx -N \exp\left(\frac{ab C_0 w_0^{(1)}}{N + uM}\right) \left(\frac{ab C_1 w_1^{(1)}}{N + Mu}\right), \quad (63)$$

and

$$y_{-1} \approx -N \exp\left(\frac{ab C_0 w_0^{(1)}}{N + uM}\right) \left(\frac{ab C_{-1} w_{-1}^{(1)}}{N + Mu}\right). \quad (64)$$

We are now able to approximate the constant terms in each of our Fourier series. From (52) and (53), we have

$$x_0 \approx \frac{M g_2 (g_2 + n) w_0^{(2)}}{ac \left(Q_2 n - (g_2 + n) w_0^{(2)}\right)}. \quad (65)$$

This implies that

$$0 \leq w_0^{(2)} \leq \frac{acnQ_2}{(g_2 + ac)(g_2 + n)}. \quad (66)$$

Furthermore,

$$w_0^{(1)} \approx \frac{N + Mu}{ab C_0 u} \left(\frac{ab |C_0| w_0^{(2)}}{M} + \ln \left(1 - \frac{g_2 (g_2 + n) w_0^{(2)}}{ac \left(Q_2 n - (g_2 + n) w_0^{(2)}\right)} \right) \right). \quad (67)$$

We note here that, for realistic C_0 such that $ab C_0 > 1$, $w_0^{(1)}$ is a monotonically-increasing function of $w_0^{(2)}$.

Moreover,

$$\frac{y_0 + (u + v)x_0}{N + (u + v)M} + \frac{y_0 + (u - v)x_0}{N + (u - v)M} \approx \frac{2g_1 (g_1 + n) w_0^{(1)}}{ac \left(nQ_1 - (g_1 + n)w_0^{(1)}\right)}. \quad (68)$$

Substituting (62), (65), and (67) into (68), we obtain a single nonlinear equation for $w_0^{(2)}$, arriving at the equation in the statement of Theorem 4.1. For each solution $w_0^{(2)}$ of (38), we can obtain a unique solution for the constant term in every other Fourier series: (67) yields $w_0^{(2)}$, (50) and (51) yield the constant terms in the Fourier series of S_{m1}^* , S_{m2}^* , E_{m1}^* , and E_{m2}^* , and (59) and (62) yields x_0 and y_0 .

Given an approximation for the constant terms of the Fourier series, we now outline an analytical method for *uniquely* approximating the coefficients associated with the *non-constant* terms.

We first make the change of variables

$$w_s^{(2)} := w_1^{(2)} + w_{-1}^{(2)}, \quad w_d^{(2)} := \mathbf{i} \cdot (w_1^{(2)} - w_{-1}^{(2)})$$

for simplicity, and consider (52), which becomes

$$\begin{aligned} \frac{g_2(g_2 + n)(w_0^{(2)} + w_s^{(2)}) + (2g_2 + n)(w_d^{(2)}) - w_s^{(2)}}{nQ_2 - (g_2 + n)(w_0^{(2)} + w_s^{(2)}) - (w_d^{(2)})} &= \\ \frac{g_2(g_2 + n)(w_0^{(2)} + w_d^{(2)}) - (2g_2 + n)(w_s^{(2)}) - (w_d^{(2)})}{nQ_2 - (g_2 + n)(w_0^{(2)} + w_d^{(2)}) + w_s^{(2)}} &= \\ \frac{g_2(g_2 + n)(w_0^{(2)} - w_s^{(2)}) - (2g_2 + n)(w_d^{(2)}) + w_s^{(2)}}{nQ_2 - (g_2 + n)(w_0^{(2)} - w_s^{(2)}) + (w_d^{(2)})}. \end{aligned} \quad (69)$$

Now considering (60) and (61), we note that, since

$$\exp\left(\frac{uab C_0 w_0^{(1)}}{N + Mu}\right) \exp\left(\frac{ab C_0 w_0^{(2)}}{M}\right) < 1,$$

and $C_1, C_{-1} \ll 1$ for sufficiently-small ω ,

$$x_1 \ll w_1^{(1)}, w_1^{(2)} \ll 1, \quad x_{-1} \ll w_{-1}^{(1)}, w_{-1}^{(2)} \ll 1.$$

Hence, we can approximate $w_s^{(2)}, w_d^{(2)} \in \mathbb{R}$ by a real solution of the system of two quadratic equations following from (69). This system can be rewritten as a single quartic for $w_s^{(2)}$, which can be shown to possess two real roots by Descartes' rule of signs, where one is extraneous (a solution $\{w_{se}^{(2)}, w_{de}^{(2)}\}$ satisfying $nQ_2 - (g_2 + n)(w_0^{(2)} + w_{de}^{(2)}) + w_{se}^{(2)} = 0$).

Once we have obtained $w_1^{(2)}, w_{-1}^{(2)}$, we can determine $w_1^{(1)}, w_{-1}^{(1)}$ similarly, using the two quadratic equations formed by substituting (63) and (64) into (53) and the previously-determined values for $w_0^{(1)}$ and y_0 . From here, the remaining coefficients follow. \square

The derivation preceding (66) in Section 4.1 indicates that all (biologically-realistic) solutions for $w_0^{(2)}$ are in the range $0 < w_0^{(2)} < \frac{acnQ_2}{(g_2+ac)(g_2+n)}$. We now turn to analyzing when (38) has *endemic* solutions in the interval above.

Appendix B: Necessary and Sufficient Conditions for (38) To Have No Endemic Solutions

We prove the following result:

Theorem 4.2. *For sufficiently-small $|v|$ and sufficiently-large ω , a necessary condition for (38) to have no nonzero solutions is*

$$\frac{Mg_2(g_2 + n)}{a^2bcn|C_0|Q_2} > 1. \quad (70)$$

A stronger, sufficient condition is

$$\frac{Mg_2(g_2 + n)}{Q_2} \left(\frac{1}{a^2bcn|C_0|} - \frac{Q_1Mu}{2g_1(g_1 + n)(N + Mu)} \left(\frac{u + v}{N + (u + v)M} + \frac{u - v}{N + (u - v)M} \right) \right) > 1. \quad (71)$$

Proof of Theorem 4.2. We begin with the proof of the sufficient condition. Since

$$F(W) := \frac{N - N \exp\left(\frac{ab|C_0|A(W)}{N + Mu}\right) + \frac{M(u+v)g_2(g_2+n)W}{ac(Q_2n - (g_2+n)W)}}{N + (u + v)M} + \frac{N - N \exp\left(\frac{ab|C_0|A(W)}{N + Mu}\right) + \frac{M(u-v)g_2(g_2+n)W}{ac(Q_2n - (g_2+n)W)}}{N - (u + v)M} - \frac{2g_1A(W)(g_1 + n)}{acnQ_1} > 0 \quad (72)$$

when W is a non-negative solution of (38), two sufficient conditions for (38) to have no nontrivial roots are

$$\begin{aligned} & \frac{N - N \exp\left(\frac{abC_0A(W)}{N + Mu}\right)}{N + (u + v)M} + \frac{N - N \exp\left(\frac{ab|C_0|A(W)}{N + Mu}\right)}{N + (u - v)M} < 0; \\ & \frac{M(u + v)g_2(g_2 + n)W}{ac(N + (u + v)M)(Q_2n - (g_2 + n)W)} + \frac{M(u - v)g_2(g_2 + n)W}{ac(N - (u + v)M)(Q_2n - (g_2 + n)W)} - \frac{2g_1A(W)(g_1 + n)}{acnQ_1} < 0 \end{aligned} \quad (73)$$

for all $W \in (0, \frac{acnQ_2}{(g_2+ac)(g_2+n)})$.

Since $A(0) = 0$, the first condition holds if $A'(W) > 0$. The second condition holds if

$$\begin{aligned} \frac{2g_1(g_1 + n)}{acnQ_1}A'(W) &> \left(\frac{u + v}{N + (u + v)M} + \frac{u - v}{N + (u - v)M} \right) \\ &\left(\frac{Mg_2(g_2 + n)}{ac(Q_2n - (g_2 + n)W)} + \frac{Mg_2(g_2 + n)^2W}{ac(Q_2n - (g_2 + n)W)^2} \right), \end{aligned} \quad (74)$$

meaning that

$$\begin{aligned} & \frac{2g_1(g_1 + n)}{acnQ_1} \frac{N + Mu}{abC_0u} \left(\frac{ab|C_0|}{M} - \frac{g_2(g_2 + n)(Q_2n - (g_2 + n)W) + g_2(g_2 + n)^2W}{(Q_2n - (g_2 + n)W)(acnQ_2 - W(g_2 + ac)(g_2 + n))} \right) > \\ & \left(\frac{M(u + v)}{(N + (u + v)M)} + \frac{M(u - v)}{N - (u + v)M} \right) \left(\frac{g_2(g_2 + n)}{ac(nQ_2 - (g_2 + n)W)} \right) \left(1 + \frac{(g_2 + n)W}{nQ_2 - (g_2 + n)W} \right). \end{aligned} \quad (75)$$

This brings us to the relation

$$-nQ_2g_2(g_2+n) \left(\frac{M(u+v)}{(N+(u+v)M)} + \frac{M(u-v)}{N-(u+v)M} \right) + \frac{2g_1(g_1+n)(N+Mu)}{nQ_1 ab C_0 u} \left(\frac{ab |C_0| (nQ_2 - (g_2+n)W)^2}{M} - \frac{g_2(g_2+n)(Q_2n - (g_2+n)W) + g_2(g_2+n)^2W}{ac} \right) > 0. \quad (76)$$

Since the left hand side is a monotonically-increasing function of W , we obtain the sufficient condition

$$-nQ_2g_2(g_2+n) \left(\frac{M(u+v)}{(N+(u+v)M)} + \frac{M(u-v)}{N-(u+v)M} \right) + \frac{2g_1(g_1+n)(N+Mu)}{nQ_1 ab C_0 u} \left(\frac{ab |C_0| (nQ_2)^2}{M} - \frac{g_2(g_2+n)(Q_2n)}{ac} \right) > 0, \quad (77)$$

from where condition (36) in Theorem 4.2 follows.

We now address the necessary condition. If

$$F(W) := -\frac{N - N \exp\left(\frac{ab|C_0|A(W)}{N+Mu}\right)}{N + (u+v)M} - \frac{N - N \exp\left(\frac{ab|C_0|A(W)}{N+Mu}\right)}{N + (u-v)M} + \frac{2g_1A(W)(g_1+n)}{ac(nQ_1 - (g_1+n)A(W))} < 0 \quad (78)$$

for some $0 < W < \frac{acnQ_2}{(g_2+ac)(g_2+n)}$, then, since

$$G(W) := \frac{M(u+v)g_2(g_2+n)W}{ac(N+(u+v)M)(Q_2n - (g_2+n)W)} + \frac{M(u-v)g_2(g_2+n)W}{ac(N+(u-v)M)(Q_2n - (g_2+n)W)} > 0 \quad (79)$$

for all $0 < W \leq \frac{acnQ_2}{(g_2+ac)(g_2+n)}$ and $F(W) > G(W)$ for W such that

$$0 < \frac{acnQ_2}{(g_2+ac)(g_2+n)} - W \ll 1,$$

$F(W)$ and $G(W)$ must intersect at a point $0 < W < \frac{acnQ_2}{(g_2+ac)(g_2+n)}$.

As a result, if $A(W) < 0$ for some $W \in (0, \frac{acnQ_2}{(g_2+ac)(g_2+n)})$, (38) must possess a positive, biologically-realistic solution for $w_0^{(2)}$. Given that $A''(W) > 0$ for all W in the interval in question, a necessary condition for (38) to have no solutions in the interval $(0, \frac{acnQ_2}{(g_2+ac)(g_2+n)})$ is the condition $A'(W) > 0$, from where (35) follows. \square

Appendix C: R_0 in the case of an isolated Patch 2 population of density M

In this case, the system (22) becomes:

$$\begin{aligned}\frac{dS_{m2}}{dt} &= g_2 Q_2 - \frac{ac I_M}{M} S_{m2} - g_2 S_{m2}; \\ \frac{dE_{m2}}{dt} &= \frac{ac I_M}{M} S_{m2} - (g_2 + n) E_{m2}; \\ \frac{dI_{m2}}{dt} &= n E_{m2} - g_2 I_{m2}; \\ I_M &= M - M \exp\left(\int_0^t \left(\frac{ab I_{m2}(\tau)}{M}\right) f(t - \tau) d\tau\right);\end{aligned}\tag{80}$$

with initial conditions

$$S_{m2}(0) = S_{m2}^{(0)}; E_{m2}(0) = E_{m2}^{(0)}; I_{m2}(0) = I_{m2}^{(0)}; I_M(0) = 0.$$

Letting $I_{m2,t} = I_{m2}(t - \phi)$, $\phi \in [-t, 0]$ (such that $I_{m2,t}$ is the *history* of I_{m2}) we find that

$$\begin{pmatrix} \frac{d}{dt} S_{m2} \\ \frac{d}{dt} E_{m2} \\ \frac{d}{dt} I_{m2} \end{pmatrix} = \mathbf{J}(S_{m2}(t), E_{m2}(t), I_{m2,t}),$$

where

$$\mathbf{J}(S_{m2}, E_{m2}, I_{m2,t}) = \begin{pmatrix} g_2 Q_2 - ac S_{m2} + ac \exp\left(\int_0^t \left(\frac{ab I_{m2}(\tau)}{M}\right) f(t - \tau) d\tau\right) S_{m2} - g_2 S_{m2} \\ ac S_{m2} - ac \exp\left(\int_0^t \left(\frac{ab I_{m2}(\tau)}{M}\right) f(t - \tau) d\tau\right) S_{m2} - (g_2 + n) E_{m2} \\ n E_{m2} - g_2 I_{m2} \end{pmatrix}.$$

The Fréchet derivative of \mathbf{J} evaluated at the DFE is

$$DQ(Q_2, 0, 0) \begin{pmatrix} S \\ E \\ I \end{pmatrix} = \begin{pmatrix} -g_2 S + ac Q_2 \left(\int_0^t \left(\frac{ab}{M}\right) f(t - \tau) d\tau\right) I \\ -(g_2 + n) E - ac Q_2 \left(\int_0^t \left(\frac{ab}{M}\right) f(t - \tau) d\tau\right) I \\ n E - g_2 I \end{pmatrix}.\tag{81}$$

By Theorem 4.7 in Diekmann and Gyllenberg [12], the characteristic equation of (80) is equivalent to

$$\det \begin{pmatrix} -g_2 - \lambda & 0 & ac Q_2 \frac{ab C_0}{M} \\ 0 & -g_2 - n - \lambda & -ac Q_2 \frac{ab C_0}{M} \\ 0 & n & -g_2 - \lambda \end{pmatrix} = 0,$$

where $C_0 := \lim_{t \rightarrow \infty} \int_0^t F(\tau) d\tau$ is defined in (27). The DFE is locally exponentially stable (which corresponds to the $R_0 < 1$ case) if the characteristic equation has all negative roots, and unstable otherwise (which corresponds to the $R_0 > 1$ case). Simplifying the left hand side and using $C_0 < 0$, we obtain

$$(-g_2 - \lambda) \left((-g_2 - n - \lambda)(-g_2 - \lambda) - nac Q_2 \frac{ab |C_0|}{M} \right) = 0,$$

which yields that the characteristic equation has all negative roots if and only if

$$\frac{a^2bcn |C_0| Q_2}{Mg_2(g_2 + n)} < 1.$$

It follows that

$$R_0 = \frac{a^2bcn |C_0| Q_2}{Mg_2(g_2 + n)} = \underbrace{(ab)}_{\substack{\text{infectious} \\ \text{bite rate per} \\ \text{infectious} \\ \text{mosquito}}} \cdot \underbrace{\frac{Q_2}{M}}_{\substack{\text{mosquito} \\ \text{to human} \\ \text{ratio}}} \cdot \underbrace{|C_0|}_{\substack{\text{expected} \\ \text{length of} \\ \text{infection} \\ \text{after 1 bite}}} \cdot \underbrace{(ac)}_{\substack{\text{infecting} \\ \text{bite rate per} \\ \text{susceptible} \\ \text{mosquito}}} \cdot \underbrace{\frac{1}{g_2 + n}}_{\substack{\text{expected} \\ \text{time mosquito} \\ \text{exposed}}} \cdot \underbrace{\frac{n}{g_2}}_{\substack{\text{sporogyny to} \\ \text{death rate} \\ \text{ratio}}}$$

We note that the same result could be obtained by retracing Appendices A and B with u, v both set to zero (in this case, the lower and upper bounds on R_0 in (37) align).

Funding

J.A. Flegg’s research is supported by the Australian Research Council (DP200100747, FT210100034) and the National Health and Medical Research Council (APP2019093).

Data availability

Data sharing not applicable to this article as no datasets were generated or analysed during the current study.

References

- [1] Nicole L Achee, Michael J Bangs, Robert Farlow, Gerry F Killeen, Steve Lindsay, James G Logan, Sarah J Moore, Mark Rowland, Kevin Sweeney, Steve J Torr, et al. Spatial repellents: from discovery and development to evidence-based validation. *Malaria Journal*, 11:1–9, 2012.
- [2] Sebastian Anița, Vincenzo Capasso, and Gabriel Dimitriu. Regional control for a spatially structured malaria model. *Mathematical Methods in the Applied Sciences*, 42(8):2909–2933, 2019.
- [3] Md Nurul Anwar, Roslyn I Hickson, Somya Mehra, James M McCaw, and Jennifer A Flegg. A multiscale mathematical model of plasmodium vivax transmission. *Bulletin of Mathematical Biology*, 84(8):81, 2022.
- [4] Pierre Auger, Etienne Kouokam, Gauthier Sallet, Maurice Tchuenté, and Berge Tsanou. The ross–macdonald model in a patchy environment. *Mathematical biosciences*, 216(2):123–131, 2008.

- [5] Melanie Bannister-Tyrrell, Charlotte Gryseels, Suon Sokha, Lim Dara, Noan Sereiboth, Nicola James, Boukheng Thavrin, Po Ly, Kheang Soy Ty, Koen Peeters Grietens, et al. Forest goers and multidrug-resistant malaria in cambodia: an ethnographic study. *The American journal of tropical medicine and hygiene*, 100(5):1170, 2019.
- [6] Elisabeth Baum, Jetsumon Sattabongkot, Jeeraphat Sirichaisinthop, Kirakorn Kiat-tibutr, Aarti Jain, Omid Taghavian, Ming-Chieh Lee, D Huw Davies, Liwang Cui, Philip L Felgner, et al. Common asymptomatic and submicroscopic malaria infections in western thailand revealed in longitudinal molecular and serological studies: a challenge to malaria elimination. *Malaria journal*, 15(1):1–15, 2016.
- [7] Ajay R Bharti, Raul Chuquiyaauri, Kimberly C Brouwer, Jeffrey Stancil, Jessica Lin, Alejandro Llanos-Cuentas, and Joseph M Vinetz. Experimental infection of the neotropical malaria vector anopheles darlingi by human patient-derived plasmodium vivax in the peruvian amazon. *The American journal of tropical medicine and hygiene*, 75(4):610, 2006.
- [8] Srean Chhim, Patrice Piola, Tambri Housen, Vincent Herbreteau, and Bunkea Tol. Malaria in cambodia: a retrospective analysis of a changing epidemiology 2006–2019. *International Journal of Environmental Research and Public Health*, 18(4):1960, 2021.
- [9] William E Collins and Geoffrey M Jeffery. Primaquine resistance in plasmodium vivax. *The American journal of tropical medicine and hygiene*, 55(3):243–249, 1996.
- [10] William E Collins, Geoffrey M Jeffery, and Jacquelin M Roberts. A retrospective examination of anemia during infection of humans with plasmodium vivax. *The American journal of tropical medicine and hygiene*, 68(4):410–412, 2003.
- [11] Jeffrey J DaCunha and John M Davis. A unified floquet theory for discrete, continuous, and hybrid periodic linear systems. *Journal of Differential Equations*, 251(11):2987–3027, 2011.
- [12] Odo Diekmann and Mats Gyllenberg. Equations with infinite delay: blending the abstract and the concrete. *Journal of differential equations*, 252(2):819–851, 2012.
- [13] Lies Durnez, Sokny Mao, Leen Denis, Patricia Roelants, Tho Sochantha, and Marc Coosemans. Outdoor malaria transmission in forested villages of cambodia. *Malaria journal*, 12:1–14, 2013.
- [14] Jennifer E Frank. Diagnosis and management of g6pd deficiency. *American family physician*, 72(7):1277–1282, 2005.
- [15] Daozhou Gao and Shigui Ruan. A multipatch malaria model with logistic growth populations. *SIAM journal on applied mathematics*, 72(3):819–841, 2012.
- [16] C Garrett-Jones. The human blood index of malaria vectors in relation to epidemiological assessment. *Bulletin of the World Health Organization*, 30(2):241, 1964.

- [17] Peter W Gething, Thomas P Van Boeckel, David L Smith, Carlos A Guerra, Anand P Patil, Robert W Snow, and Simon I Hay. Modelling the global constraints of temperature on transmission of plasmodium falciparum and p. vivax. *Parasites & Vectors*, 4(1):92, 2011.
- [18] María-Eugenia Grillet, Mayida El Souki, Francisco Laguna, and José Rafael León. The periodicity of plasmodium vivax and plasmodium falciparum in venezuela. *Acta Tropica*, 129:52–60, 2014.
- [19] Weidong Gu, James L Regens, John C Beier, and Robert J Novak. Source reduction of mosquito larval habitats has unexpected consequences on malaria transmission. *Proceedings of the National Academy of Sciences*, 103(46):17560–17563, 2006.
- [20] Monnaphat Jongdeepsaisal, Mom Ean, Chhoeun Heng, Thoek Buntau, Rupam Tripura, James J Callery, Thomas J Peto, Franca Conradis-Jansen, Lorenz von Seidlein, Panarasri Khonputsra, et al. Acceptability and feasibility of malaria prophylaxis for forest goers: findings from a qualitative study in cambodia. *Malaria Journal*, 20(1):1–15, 2021.
- [21] Uriel Kitron and Andrew Spielman. Suppression of transmission of malaria through source reduction: antianopheline measures applied in israel, the united states, and italy. *Reviews of infectious diseases*, 11(3):391–406, 1989.
- [22] Waldemar Klassen. Introduction: development of the sterile insect technique for african malaria vectors, 2009.
- [23] Amber Kunkel, Chea Nguon, Sophea Iv, Srean Chhim, Dom Peov, Phanith Kong, Saorin Kim, Sarun Im, Mark Debackere, Nimol Khim, et al. Choosing interventions to eliminate forest malaria: preliminary results of two operational research studies inside cambodian forests. *Malaria journal*, 20(1):1–13, 2021.
- [24] Dolie D Laishram, Patrick L Sutton, Nutan Nanda, Vijay L Sharma, Ranbir C Sobti, Jane M Carlton, and Hema Joshi. The complexities of malaria disease manifestations with a focus on asymptomatic malaria. *Malaria journal*, 11(1):1–15, 2012.
- [25] Somya Mehra, James M McCaw, and Peter G Taylor. Superinfection and the hypnozoite reservoir for plasmodium vivax: a general framework. *arXiv preprint arXiv:2306.14329*, 2023.
- [26] Somya Mehra, Eva Stadler, David Khoury, James M McCaw, and Jennifer A Flegg. Hypnozoite dynamics for plasmodium vivax malaria: the epidemiological effects of radical cure. *Journal of Theoretical Biology*, 537:111014, 2022.
- [27] Janet T Midega, Charles M Mbogo, Henry Mwambi, Michael D Wilson, Gordon Ojwang, Joseph M Mwangangi, Joseph G Nzovu, John I Githure, Guiyun Yan, and John C Beier. Estimating dispersal and survival of anopheles gambiae and anopheles funestus along the kenyan coast by using mark–release–recapture methods. *Journal of medical entomology*, 44(6):923–929, 2007.

- [28] April Monroe, Nana Aba Williams, Sheila Ogoma, Corine Karema, and Fredros Okumu. Reflections on the 2021 world malaria report and the future of malaria control, 2022.
- [29] Francois M Moukam Kakmeni, Ritter YA Guimapi, Frank T Ndjomatchoua, Sansoa A Pedro, James Mutunga, and Henri EZ Tonnang. Spatial panorama of malaria prevalence in africa under climate change and interventions scenarios. *International journal of health geographics*, 17(1):1–13, 2018.
- [30] Ingemar Nasell. *Hybrid models of tropical infections*, volume 59. Springer Science & Business Media, 2013.
- [31] World Health Organization et al. *World malaria report 2022*. World Health Organization, 2022.
- [32] Hans J Overgaard, Barbara Ekbom, Wannapa Suwonkerd, and Masahiro Takagi. Effect of landscape structure on anopheline mosquito density and diversity in northern thailand: Implications for malaria transmission and control. *Landscape ecology*, 18:605–619, 2003.
- [33] Sochea Phok, Saysana Phanalasy, Si Thu Thein, and Asawin Likhitsup. Private sector opportunities and threats to achieving malaria elimination in the greater mekong subregion: results from malaria outlet surveys in cambodia, the lao pdr, myanmar, and thailand. *Malaria journal*, 16:1–22, 2017.
- [34] Sochea Phok, Kemi Tesfazghi, Andy Tompsett, Boukheng Thavrine, Po Ly, Saad El-Din Hassan, Avery Avrakotos, Jim Malster, and Erica Felker-Kantor. Behavioural determinants of malaria risk, prevention, and care-seeking behaviours among forest-goers in cambodia. *Malaria Journal*, 21(1):362, 2022.
- [35] Olivia Prosper, Nick Ruktanonchai, and Maia Martcheva. Assessing the role of spatial heterogeneity and human movement in malaria dynamics and control. *Journal of Theoretical Biology*, 303:1–14, 2012.
- [36] Raju Ranjha and Amit Sharma. Forest malaria: the prevailing obstacle for malaria control and elimination in india. *BMJ Global Health*, 6(5):e005391, 2021.
- [37] Diego J Rodríguez and Lourdes Torres-Sorando. Models of infectious diseases in spatially heterogeneous environments. *Bulletin of Mathematical Biology*, 63(3):547–571, 2001.
- [38] Adam Saddler, Katharina S Kreppel, Nakul Chitnis, Thomas A Smith, Adrian Denz, Jason D Moore, Mgeni M Tambwe, and Sarah J Moore. The development and evaluation of a self-marking unit to estimate malaria vector survival and dispersal distance. *Malaria journal*, 18(1):1–14, 2019.
- [39] Mirco Sandfort, Amélie Vantaux, Saorin Kim, Thomas Obadia, Anaïs Pepey, Soazic Gardais, Nimol Khim, Dysoley Lek, Michael White, Leanne J Robinson, et al. Forest malaria in cambodia: the occupational and spatial clustering of plasmodium vivax and plasmodium falciparum infection risk in a cross-sectional survey in mondulkiri province, cambodia. *Malaria journal*, 19:1–12, 2020.

- [40] David L Smith, Chris J Drakeley, Christinah Chiyaka, and Simon I Hay. A quantitative analysis of transmission efficiency versus intensity for malaria. *Nature communications*, 1(1):108, 2010.
- [41] Peter Starzengruber, Hans-Peter Fuehrer, Benedikt Ley, Kamala Thriemer, Paul Swoboda, Verena Elisabeth Habler, Mariella Jung, Wolfgang Graninger, Wasif A Khan, Rashidul Haque, et al. High prevalence of asymptomatic malaria in south-eastern bangladesh. *Malaria journal*, 13:1–10, 2014.
- [42] Cheong H Tan, Indra Vythilingam, Asmad Matusop, Seng T Chan, and Balbir Singh. Bionomics of anopheles latens in kapit, sarawak, malaysian borneo in relation to the transmission of zoonotic simian malaria parasite plasmodium knowlesi. *Malaria journal*, 7(1):1–8, 2008.
- [43] Michael T White, Stephan Karl, Katherine E Battle, Simon I Hay, Ivo Mueller, and Azra C Ghani. Modelling the contribution of the hypnozoite reservoir to plasmodium vivax transmission. *Elife*, 3:e04692, 2014.
- [44] Michael T White, George Shirreff, Stephan Karl, Azra C Ghani, and Ivo Mueller. Variation in relapse frequency and the transmission potential of plasmodium vivax malaria. *Proceedings of the Royal Society B: Biological Sciences*, 283(1827):20160048, 2016.